1967

The differential capacity of the electrical double layer at the silver iodide-aqueous solution interface

David Morton Barshatky
Iowa State University

67-8901

BARSHATKY, David Morton, 1939-

THE DIFFERENTIAL CAPACITY OF THE ELECTRICAL DOUBLE LAYER AT THE SILVER IODIDE-AQUEOUS SOLUTION INTERFACE.

Iowa State University of Science and Technology, Ph.D., 1967
Chemistry, physical

University Microfilms, Inc., Ann Arbor, Michigan

THE DIFFERENTIAL CAPACITY OF THE ELECTRICAL DOUBLE LAYER AT THE SILVER IODIDE–AQUEOUS SOLUTION INTERFACE

by

David Morton Barshatky

A Dissertation Submitted to the
Graduate Faculty in Partial Fulfillment of
The Requirements for the Degree of
DOCTOR OF PHILOSOPHY

Major Subject: Physical Chemistry

Approved:

Signature was redacted for privacy.

In Charge of Major Work

Signature was redacted for privacy.

Head of Major Department

Signature was redacted for privacy.

Dean of Graduate College

Iowa State University
Of Science and Technology
Ames, Iowa

1967

TABLE OF CONTENTS

INTRODUCTION

During the last two decades there has been an extensive investigation of the properties of the electrical double layer occurring at charged interfaces. The origin of the double layer depends on whether the interface is polarizable or nonpolarizable.

Consider a metal-solution interface. Let a reference electrode be inserted in solution and let an electromotive force (e.m.f.) be applied between the metal and reference electrodes by use of a potentiometer. The potential range should be wide but limited to the extent that a negligible charge is transferred across the interface. Such an interface is said to be polarizable. Upon application of this e.m.f. a surplus (or deficit) of electrons occurs on the metal surface via delivery (or removal) of electrons by the potentiometer while a deficit (or surplus) of electrons occurs in the solution via oxidation (or reduction) of a particular ion. Then in simplified form the double layer at a polarizable interface consists of a layer of electronic charge on the metal surface, a charge distribution of ions containing a net charge equal (but opposite in sign) to that on the metal in the solution region adjacent to the metal, and a layer of solvent molecules between the metal and the ionic charge distribution. The mercury-solution interface best represents such a system.

Consider a reversible electrode-solution interface. This is illustrated by the silver iodide-solution interface. Some Ag^+ and I^- ions will adsorb on the AgI surface resulting in the establishment of a net charge on the surface and an equal but opposite charge in solution. Such an

interface is said to be nonpolarizable since a charge has been transferred across the interface. Note here that the charge and potential depend on the concentration of Ag^+ (or I^-) in the solution bulk. Then in simplified form the double layer at a nonpolarizable interface such as the AgI-solution interface consists of a net ionic charge on the AgI surface, a charge distribution of ions containing a net charge equal (but opposite in sign) to that on the surface in the solution region adjacent to the AgI and a layer of solvent molecules between the AgI surface and the ionic charge distribution.

In general the above mentioned layer of solvent molecules is called the compact or Stern layer while the ionic charge distribution in the solution is called the diffuse or Gouy layer. The plane through the distance from the surface of closest approach of the electrical center of the ions in the diffuse layer is the boundary between the Stern and diffuse layers and is called the outer Helmholtz plane. This double layer model is called the Stern-Grahame model. When adsorption of ions occurs in the Stern layer the above simple model has to be modified. An ion without a solvent sheath on the side of the ion adjacent to the solid surface is said to be specifically adsorbed in the Stern layer. Significant specific adsorption is frequently encountered with anions but infrequently with cations; this reflects the greater ease of partial dehydration of the anions.

Let ψ_o denote the relative potential at the surface ($x = 0$) and ψ_δ the relative potential at the outer Helmholtz plane ($x = \delta$). The relative potential in the solution bulk is zero. Let σ_o denote the charge density

on the solid surface. Suppose there is no specific adsorption. Then it can be seen that the Stern and diffuse layers behave as differential capacitors in series in which

$$1/\varkappa = 1/C_c + 1/C_g \qquad (1)$$

where C_c is the Stern capacity, C_g is the diffuse capacity, and $\varkappa$ the double layer capacity. We have

$$\varkappa = d\sigma_o/d\,\psi_o \qquad (1')$$

$$C_c = d\sigma_o/d(\psi_o - \psi_\delta) \qquad (2)$$

$$C_g = d\sigma_o/d\,\psi_\delta \qquad (3)$$

In these formulae capacitances per unit area are considered in order to utilize parameters independent of surface area.

Expressions for the dependence of the charge density and differential capacity of the diffuse layer on the surface potential were derived by Gouy and Chapman (1909-13) by use of a Boltzman distribution of ions. Incorrectly they assumed the diffuse layer began at the surface (x = 0). The charge density σ_g in coulombs/cm^2 of the diffuse layer containing ions of the same valence is

$$\sigma_g = -\left[\frac{1}{9 \times 10^{11}}\right]^{1/2} \left[\frac{2n_o kT\epsilon}{\pi}\right]^{1/2} \sinh \frac{ze\,\psi_\delta}{2kT}$$

where n_o is the number of ions per cm^3 in the solution bulk, ϵ is the solvent dielectric constant, k is the Boltzmann constant in joules/deg

molecule, z is the ion valence, e is the electronic charge in coulombs and ψ_δ is in volts. By differentiation of σ_g with respect to ψ_δ the differential capacity C_g in farads/cm^2 of the diffuse layer is obtained.

$$C_g = \left[\frac{1}{9 \times 10^{11}}\right]^{1/2} \left[\frac{z^2 e^2 n_o \epsilon}{2\pi kT}\right]^{1/2} \cosh \frac{ze\,\psi_\delta}{2kT} \qquad (3')$$

It is seen that C_g is independent of the properties of the surface at the interface and is a minimum at the zero point of charge (zpc), that is at $\sigma_g = 0$.

$$C_g \text{ (min)} = \left[\frac{1}{9 \times 10^{11}}\right]^{1/2} \left[\frac{z^2 e^2 n_o \epsilon}{2\pi kT}\right]^{1/2} \qquad (3'')$$

In general the capacity C_p of a parallel plate condenser in farads/cm^2 is expressed by

$$C_p = \frac{\epsilon p}{4\pi \tau_p} \quad \frac{1}{9 \times 10^{11}}$$

where τ_p is the distance between the plates in cm. Hence from Equation 3'' the characteristic thickness of the diffuse layer called the Debye length λ_D in cm is defined as

$$1/\lambda_D = (9 \times 10^{11})^{1/2} \left[\frac{8\pi z^2 e^2 n_o}{\epsilon kT}\right]^{1/2}$$

It is also seen that C_g is very small for very dilute solutions near the zero point of charge, and for sufficiently dilute solutions will be small compared to the Stern capacity. In this case Equation 1 shows that the double layer capacity will approximately equal the diffuse capacity.

In 1924 Stern (1) incorporated the charge free solvent layer in the double layer model in order to account for ionic dimensions. There is no simple dependence of the differential capacity of the Stern layer on potential. Grahame (2) employed his experimental values of the double layer capacity of the Hg-aqueous NaF solution interface and the Gouy-Chapman theory of the diffuse layer to calculate the Stern capacity at a given surface charge density from Equation 1. He found that the Stern capacity varied strongly with the surface charge and suggested that such a dependence resulted from the compression and dielectric saturation of the solvent molecules in the Stern layer by the high electric field emanating from the surface. The former causes a rise while the latter causes a drop in the Stern capacity. At any rate for concentrated solutions or at very high negative or positive potentials the diffuse capacity is large and in this case the double layer capacity will approximately equal the Stern capacity.

Briefly, the double layer model is modified as follows upon specific adsorption. Let σ_1 denote the charge density in the Stern layer due to specific adsorption.

Since $$\psi_o = \psi_o - \psi_\delta + \psi_\delta$$

then $$\frac{d\psi_o}{d\sigma_o} = \frac{d(\psi_o - \psi_\delta)}{d\sigma_o} + \frac{d\psi_d}{d\sigma_g}\frac{d\sigma_g}{d\sigma_o}$$

Hence $$\frac{1}{\chi} = \frac{1}{C_c} - \frac{1}{C_g}\frac{d\sigma_g}{d\sigma_o}$$

we have $$\sigma_o = -(\sigma_1 + \sigma_g)$$

Then differentiation with respect to σ_o yields

$$\frac{-d\sigma_g}{d\sigma_o} = 1 + \frac{d\sigma_1}{d\sigma_o}$$

Hence

$$\frac{1}{\varkappa} = \frac{1}{C_c} + \frac{1}{C_g}\left(1 + \frac{d\sigma_1}{d\sigma_o}\right) \qquad (1'')$$

It is observed that the double layer capacity $\varkappa$ values for the Hg-solution interface rise in the potential region where specific adsorption occurs. From Equation 1'' this rise is caused by an increase in the Stern capacity C_c upon specific adsorption compared to that without such adsorption and by the change of adsorption with surface charge σ_o.

Since the double layer behaves as a differential capacity much information about the structure and properties of the double layer can be obtained by measuring $\varkappa$ as a function of potential. Other approaches to the study of the double layer structure are illustrated, for example, by measurements of the surface tension γ at a Hg-solution interface as a function of potential and the measurement of the surface charge density σ at the AgI-solution interface as a function of potential. The surface tension γ is related to the surface charge density σ in the absence of specific adsorption by the Lippmann equation

$$-d\gamma = \sigma dV$$

where V is the applied e.m.f. Differentiation of the γ-V curve gives the σ-V curve which upon differentiation yields the $\varkappa$ -V curve. The above two methods were first used to elucidate double layer properties.

In 1935 Frumkin and Proskurnin (3) were the first to publish reliable

work on the direct measurement of the double layer differential capacity. They used an oscillographic technique with a low amplitude signal to study the Hg-solution interface. A low amplitude signal is required because χ itself is a function of potential. Thereafter Grahame (4) improved the alternating current (a.c.) bridge technique and published extensive double layer capacity results for the Hg-solution interface. However, such methods may not be workable for reversible interfaces. When an a.c. signal is imposed across the reversible interface a concentration gradient of the potential determining ions is set up resulting in the diffusion of these ions back and forth from the solution to the solid surface which disrupts the double layer. The resistance of a reversible electrode is usually sufficiently high that the balance point in the a.c. bridge technique cannot be obtained with accuracy. Reversible electrodes are usually somewhat rough and this results in frequency-dependent data. Such results would have to be interpreted quantitatively. As a consequence no work on reversible electrodes via the a.c. bridge technique has been successful. The first problem may be overcome by using signals of sufficiently high frequency that the polarity of the signal changes sufficiently rapidly that the ions always reverse direction before reaching the interface. The second problem may be overcome by using a reversible electrode with a relatively high conductivity. At the same time it should have a relatively wide accessible potential range and be such that studies of its double layer properties occur in the literature. The third problem may be overcome by using a very rough, relatively smooth or porous electrode. In these cases the frequency dispersion can

be quantitatively explained in terms of known quantities. With this in mind we applied the a.c. bridge technique to the AgI-aqueous solution interface to determine its differential double layer capacity as a function of potential and ionic strength. AgI has a relatively high conductivity for solids, has an accessible potential range of about 450 millivolts and double layer studies on the AgI-solution interface have been very extensive with work done by Van Laar (5), Mackor (6,7), Lyklema (8,9), Agar (10), and others.

The stability of all lyophobic colloids depends on the electrical repulsion between particles resulting from their surface charges partly screened by the diffuse double layer. Once the character of the double layer is thoroughly understood it is possible to calculate the rate of flocculation as a function of surface charge and electrolyte concentration. High precision measurements of double layer properties have so far only been available for the mercury-electrolytic solution interface, the high precision results from the use of alternating current bridge measurements in this system. In general lyophobic colloids depend for stability on ion adsorption, and in this respect the polarized mercury surface poorly represents them. Silver iodide forms excellent colloidal dispersions, and they have been widely studied. As pointed out, the silver iodide-solution interface is also a classical example of the reversible interface. It is for this reason that the development of methods for measuring electrical properties of this interface with high precision is of such fundamental importance.

MATERIALS

Water

All solutions were prepared from freshly distilled conductivity water. The conductivity water was prepared by use of a fused silica continuous double distillation column obtained from Engelhard Industries, Inc. Further details are described by Kelsh (11).

Chemicals

KNO_3 used as the electrolyte was recrystallized twice from water. $AgNO_3$ used as a titrant was reagent grade. KI used as a titrant and in preparing the AgI electrodes was recrystallized from water. AgI used to buffer the cell solution was prepared from KI and $AgNO_3$ solutions.

Inert Atmosphere

Tank nitrogen was used to flush the cell. It entered the cell through a glass filter stick which dispersed the gas in a stream of small bubbles and left the cell through a water bubbler.

Silver Iodide Electrodes

The AgI electrodes were prepared as follows. Silver wire #26 obtained from Sargent Co. was inserted through a hole in a 9 mm cork stopper which in turn had been inserted at one end of a 9 mm glass tubing. The silver wire protruded from both ends of the tube. A glue mixture of Araldite 502 Epoxy Resin (10 parts by weight) and Hardener 951 (1 part by weight) was

then used to seal carefully the end of the tube containing the cork without contaminating the exposed Ag. A schematic diagram of the electrode is shown in Figure 1.

The glue components were obtained from CIBA Products Company, Fair Lawn, New Jersey. The mixture gels in about 50 minutes at 25°C and is then cured for 3 days.

The exposed length and radius of the silver wire were measured with a measuring microscope. The silver electrode was then partly immersed in a .1 N KI solution along with a Pt electrode. The Ag electrode was connected to the positive terminal of a battery while the Pt electrode was connected to the negative terminal. An AgI deposit was then formed on the Ag electrode by electrolysis, and its thickness was estimated from the Faraday Law of electrolysis. Thus

$$m = \frac{E_w I t}{F}$$

where m is the mass deposited on the electrode, E_w is the equivalent weight of the substance formed, I is the current through the electrode and t is the time of electrolysis. Since the electrode is cylindrical the volume V_e of AgI is expressed by

$$V_e = \pi d h \tau_e$$

where d is the diameter of the cylinder, h is the length, and τ_e is the thickness of the AgI.

Then the mass m of AgI is

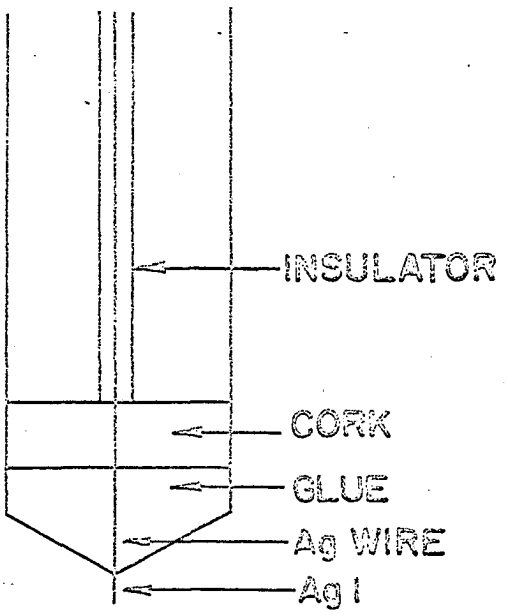

Figure 1. AgI electrode schematic

$$m = \pi dh \tau_e \rho_e$$

where ρ_e is the density of AgI.

Hence thickness τ_e is expressed by

$$\tau_e = \frac{E_w It}{\pi F dh \rho_e}$$

Using E_w = 234.8 grams/equivalent, ρ_e = 5.67 grams/cm^3, F = 9.650×10^4 coulombs/equivalent we get

$$\tau_e = \frac{1.37 \times 10^{-4}\ It}{dh}$$

The area Ae of the AgI electrode can be expressed by

$$Ae = \pi \left(dh + \frac{d^2}{4}\right)$$

Table 1 lists the geometrical characteristics of the various electrodes investigated.

The experimental cell consists of an AgI and a 1N calomel electrode in contact with an aqueous KNO_3 solution containing very dilute concentrations of Ag^+ and I^- ions. The cell can be written as

$$\text{Hg} \mid \text{Hg}_2\text{Cl}_2(s) \mid \text{KCl (1N)} \; \begin{matrix} \text{KNO}_3(C_e) \\ \text{AgNO}_3(C_{Ag^+}) \\ \text{KI}(C_{I^-}) \end{matrix} \mid \text{AgI}(s) \mid \text{Ag}$$

where C_e is the concentration of the electrolyte KNO_3, C_{Ag^+} is the concentration of Ag^+ and C_{I^-} is the concentration of I^-. The liquid junction potential remains nearly constant because the KCl concentration in the salt bridge is large compared to other concentrations at the

Table 1. The diameter d in cm, length h in cm, thickness of AgI τ_e in cm and area Ae in cm^2 for the various AgI electrodes

Electrode	d x 10^2	h x 10^1	τ_e x 10^4	Ae x 10^2
# 9	4.15	2.64	3.4	3.58
#10	4.16	2.63	4.7	3.57
#11	4.08	1.96	0.44	2.64

junction. Chloride ion contamination of the solution was minimized by making the contact between the salt bridge and the solution through a hole of such small radius that a negligible quantity/hr of Cl^- entered the solution and by placing this electrode in solution only during the small time periods when potentials were actually being measured. New solutions were used for each set of measurements. The half cell reaction in excess of Ag^+ is:

$$Hg + Cl^-(1N) \longrightarrow 1/2\ Hg_2Cl_2(s) + e^-,\ E_{cal} = -281\ mv$$

$$Ag^+ + e^- \longrightarrow Ag \qquad ,\ E^o = 799\ mv$$

$$Ag^+ + Hg + Cl^-(1N) \longrightarrow 1/2\ Hg_2Cl_2(s) + Ag$$

The cell potential E_c in excess Ag^+ is expressed by

$$E_c = E_{cal} + E^o_{Ag^+,Ag} + \frac{RT}{F} \ln a_{Ag^+}$$

where a_{Ag^+} is the activity of Ag^+ ion.

Then $$E_c = 518 + \frac{RT}{F} \ln \gamma_{Ag^+} + \frac{RT}{F} \ln C_{Ag^+}$$

where γ_{Ag^+} is the activity coefficient of Ag^+ ion.

We define

$$E^{o'}_{Ag} = 518 + \frac{RT}{F} \ln \gamma_{Ag^+}$$

Then $$E_c = E^{o'}_{Ag} + \frac{RT}{F} \ln C_{Ag^+} \qquad (4)$$

The cell reaction in excess I^- is:

$$Hg + Cl^-(1N) \longrightarrow 1/2\ Hg_2Cl_2(s) + e^- \quad , E_{cal} = -281 \text{ mv}$$

$$AgI(s) + e^- \longrightarrow Ag + I^- \quad , E^o = -152 \text{ mv}$$

$$AgI(s) + Hg + Cl^-(1N) \longrightarrow Ag + I^- + 1/2\ Hg_2Cl_2(s)$$

The cell potential E_c in excess I^- is expressed by

$$E_c = E_{cal} + E^o_{AgI,Ag} - \frac{RT}{F} \ln a_{I^-}$$

where a_{I^-} is the activity of I^- ion.

Then $$E_c = -433 - \frac{RT}{F} \ln \gamma_{I^-} - \frac{RT}{F} \ln C_{I^-}$$

where γ_{I^-} is the activity coefficient of I^- ion.

We define

$$E^{o'}_{I} = -433 - \frac{RT}{F} \ln \gamma_{I^-}$$

Then $$E_c = E^{o'}_{I} - \frac{RT}{F} \ln C_{I^-} \qquad (5)$$

Note that γ_{Ag^+} and γ_{I^-} depend only on the ionic strength of the electrolyte.

We find an expression for pK_{sp} for AgI as follows:

From Equations 4 and 5

$$E^{o'}_{Ag} - E^{o'}_{I} = - \frac{RT}{F} \ln (C_{I^-} C_{Ag^+})$$

Since $K_{sp} = C_{I^-} C_{Ag^+}$

then

$$pK_{sp} = - \log K_{sp} = \frac{F(E^{o'}_{Ag} - E^{o'}_{I})}{2.303\ RT} \tag{6}$$

The relative potential ψ is defined as

$$\psi = E_c - E_c(zpc) \tag{7}$$

where $E_c(zpc)$ denotes the cell potential at the zero point of charge, that is the cell potential at which equal amounts of Ag^+ and I^- have adsorbed on the AgI surface to give a zero net charge. In plotting double layer capacity curves the potential ψ is used as the abscissa. Actually the surface potential ψ_o should be used as the abscissa but is not accessible experimentally. ψ_o is a component of ψ, and under certain conditions they are equal. This point will be discussed later. Let $C^o_{Ag^+}$ denote the concentration of Ag^+ at the zero point of charge. Then from Equation 4

$$\psi = \frac{RT}{F} \ln \frac{C_{Ag^+}}{C^o_{Ag^+}} \tag{7'}$$

Hence ψ is positive when an excess Ag^+ has adsorbed on the AgI surface and negative for an excess of I^-. Van Laar (5) has done the most extensive and reliable study of the zero point of charge on AgI, and we shall take his value, expressed as pAg = 5.45 at the zero point of charge in dilute KNO_3 solution. We will assume there is no shift in the zero point of charge with increasing ionic strength for those we use.

Then

$$C^{o}_{Ag^+} = 3.55 \times 10^{-6} \text{ moles/liter}$$

The standard potentials $E^{o'}_{Ag}$ and $E^{o'}_{I}$ were determined at a given ionic strength by measuring the potential E_c of the above cell at various known concentrations of Ag^+ and I^- by use of a Beckman pH meter. Equation 4 is used to calculate $E^{o'}_{Ag}$ and Equation 5 is used to calculate $E^{o'}_{I}$. Once these values are known we can calculate unknown concentrations of Ag^+ and I^- at a given cell potential. The rational potential ψ at a given cell potential can also be determined. The values of $E^{o'}_{Ag}$, $E^{o'}_{I}$ and pK_{sp} for representative electrodes are listed in Table 2. They are in accord with the values determined by other workers.

Table 2. The standard cell potentials $E^{o'}_{Ag}$ and $E^{o'}_{I}$ in millivolts and pK_{sp} for various AgI electrodes

Ionic strength	Electrode	$E^{o'}_{Ag}$	$E^{o'}_{I}$	pK_{sp}
.1020	# 9	515	- 412	15.67
	#10	513	- 416	15.70
.01020	# 9	526	- 410	15.82
	#10	523	- 415	15.86
.001020	# 9	529	- 411	15.89
	#10	525	- 415	15.89

APPARATUS

The Impedance Bridge Cell

The container for the solution was formed from a 55/60 Pyrex double walled standard taper, outer. The ring seal at the bottom completed a thermostatting jacket through which water from a constant temperature bath could be circulated. A glass tube, 2 cm in diameter but tapered at the bottom was attached to an outlet at one side of the container. This tube was used to contain the reference electrode.

A 55/60 Pyrex standard taper, inner, was attached to the top of the above container. This served as a support for the various components of the cell. A platinum gauze electrode was connected to the support by a platinum wire sealed through a glass sheath, which in turn was ring-sealed to the support. The a.c. signal was applied between this electrode and the AgI electrode. A gas dispersing tube was also connected to the support by a ring seal. A Teflon plug stopcock directed the incoming gas through this tube when closed.

A 12/30 Pyrex standard taper, outer, was attached to the top of the cell support. The AgI electrode was inserted through a Teflon plug, the outside of which had been machined to fit tightly the 12/30 Pyrex standard taper, outer.

A schematic diagram of the cell is shown in Figure 2.

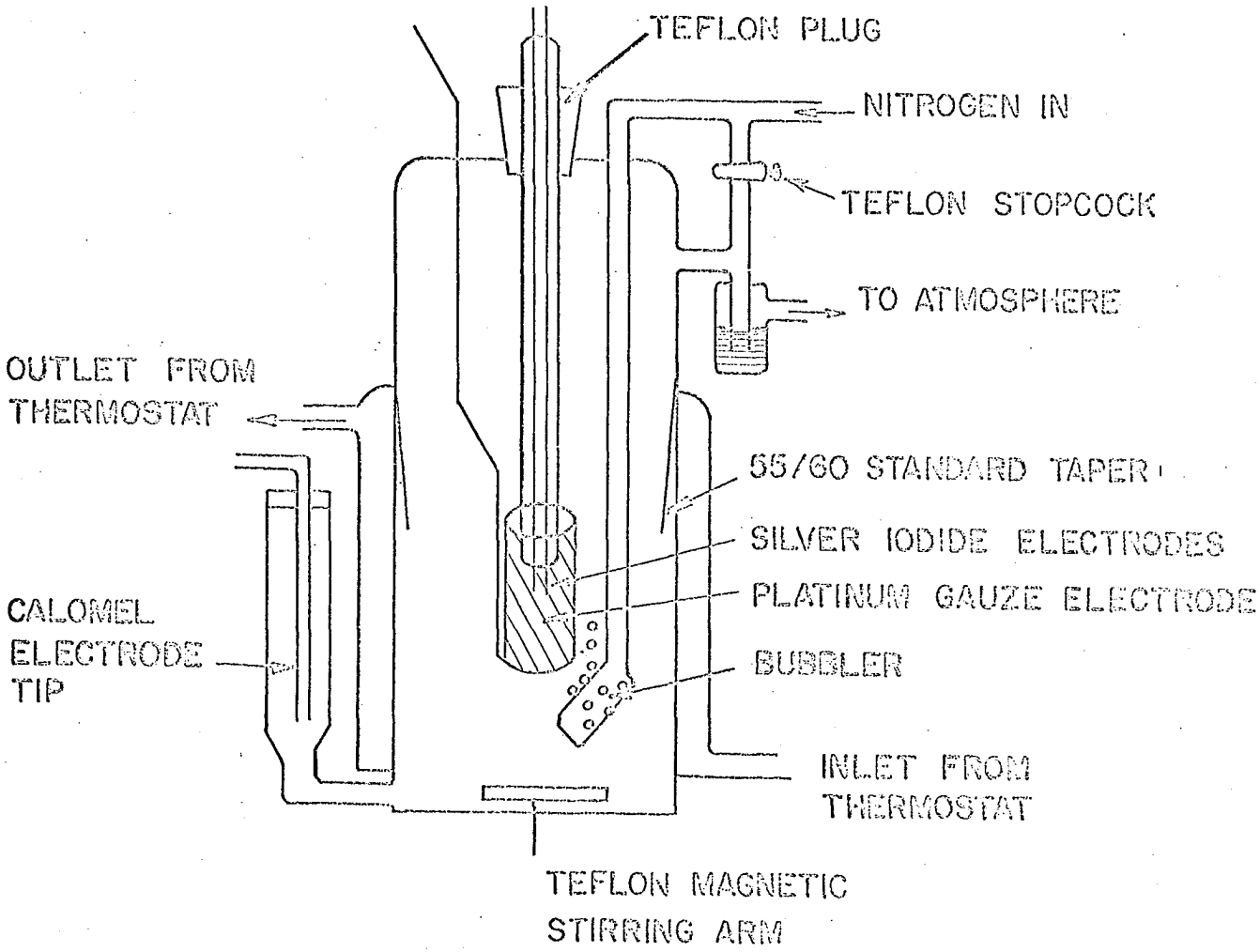

Figure 2. Impedance bridge cell schematic

Electronic Apparatus

The impedance bridge was constructed around a Leeds and Northrup Co. shielded ratio box, catalog number 1553. The ratio box contains ratio arms for a one to one impedance bridge, i.e., 2 adjacent arms of the bridge are resistors of equal magnitude. It also has a shielded step-down input transformer and a network for use in balancing the bridge. These are all enclosed in a metal case which acts as a shield. Various external pieces of equipment were connected to shielded binding posts on the box.

The input signal to the transformer in the ratio box was supplied by a Hewlett Packard Model 200 CD wide range oscillator.

The measuring arm of the bridge consisted of a Freed Transformer Co. Model 1350 decade capacitor and a non-inductively wound Leeds and Northrup Co. decade resistance, catalog number 4764, in series connection. The decade capacitor consisted of 4 decades in units of .001 μf, .01 μf and 1 μf, and a continuously variable air capacitor with a scale calibrated in units of 10 μμf with a range up to a maximum of .001 μf. The decade resistance consisted of 6 decades in units of .01, .1, 1, 10, 100, and 1000 ohms.

The output signal from the bridge needed amplification before it could be displayed on an oscilloscope and this was first furnished by a Hewlett Packard Model 450A wide band amplifier operating at a gain of 100 to 1. This signal was in turn amplified by a twin-tee narrow band amplifier designed and constructed in this laboratory.

Pairs of tees used in the measurements were constructed for use at

nominal frequencies 250, 500, 750, 1000, 2500, 5000, and 10,000 cycles per second. The amplified signal from the twin tee was put into the Y input of the oscilloscope and produced the Y displacement on the screen. A Dumont Type 304-H cathode ray oscilloscope was used.

In order to gain additional sensitivity in the measurements a phase sensitive technique was used. A second Hewlett Packard Model 450A wide band amplifier operating at a gain of 100 to 1 had its input connected to the bridge and its output to the X input of the oscilloscope so the input signal to the bridge could be amplified and used to produce the X displacement on the oscilloscope screen. These X and Y inputs produced a Lissajous figure on the screen. A horizontal straight line indicated the output signal from the bridge was zero and the bridge balanced.

A second pair of series elements similar to the above decade capacitor and decade resistance were then substituted for the cell in the bridge. The bridge was then balanced again by adjusting this second pair of elements. Such a calibration procedure is needed in order to eliminate effects due to asymmetries in the bridge network and in the electrical leads. By using identical shielded electrical leads for connecting both the cell and cell analog to the bridge terminal the impedance of the cell and the cell analog became the same.

A diagram of the bridge is shown in Figure 3.

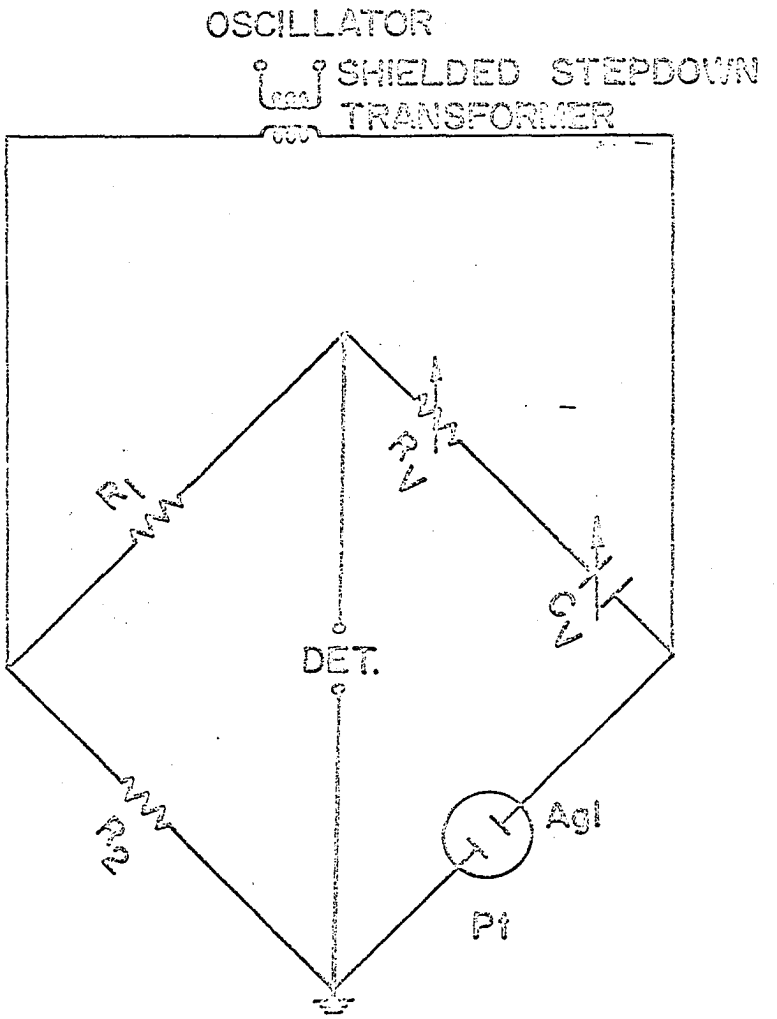

Figure 3. Impedance bridge schematic

THEORY

Consider an AgI-aqueous solution interface with an a.c. signal applied across it. The AgI surface is somewhat porous so it will consist of porous and flat, smooth parts as illustrated in Figure 4. Each pore filled with solution has an impedance Z_A which we assume is equivalent to a series combination of a capacitance C_A and resistance R_A. The impedance Z_P of all pores is the resultant of the pore impedances connected in parallel. Hence it can be represented as a series combination of a capacitance C_P and resistance R_P. The impedance at the flat part of the interface consists of the double layer capacitance C_D in parallel with its associated Faradaic impedance Z_F. The latter consists of a series combination of capacitance C_F and resistance R_F. The impedance Z_S at the entire interface is the resultant of the porous impedance Z_P connected in parallel with the flat impedance. The circuit for the AgI interface as described above is illustrated in Figure 5. Hence impedance Z_S is given by

$$\frac{1}{Z_S} = \frac{1}{Z_P} + i\omega C_D + \frac{1}{Z_F} \tag{8}$$

where

$$Z_P = R_P - \frac{i}{\omega C_P} \tag{8'}$$

$$Z_F = R_F - \frac{i}{\omega C_F} \tag{8''}$$

In the following paragraphs expressions for C_P, R_P, C_F, and R_F will be derived.

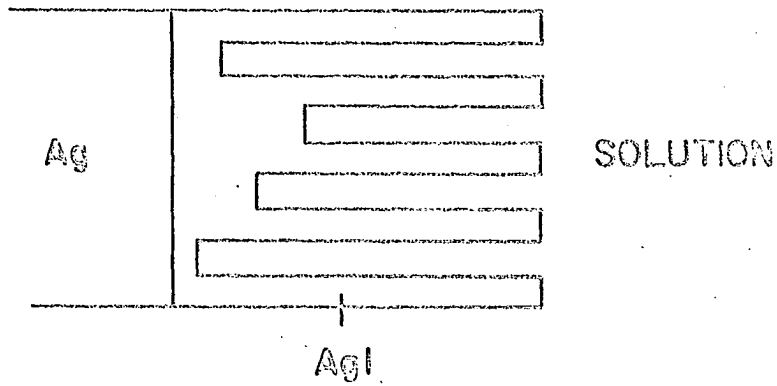

Figure 4. AgI surface schematic

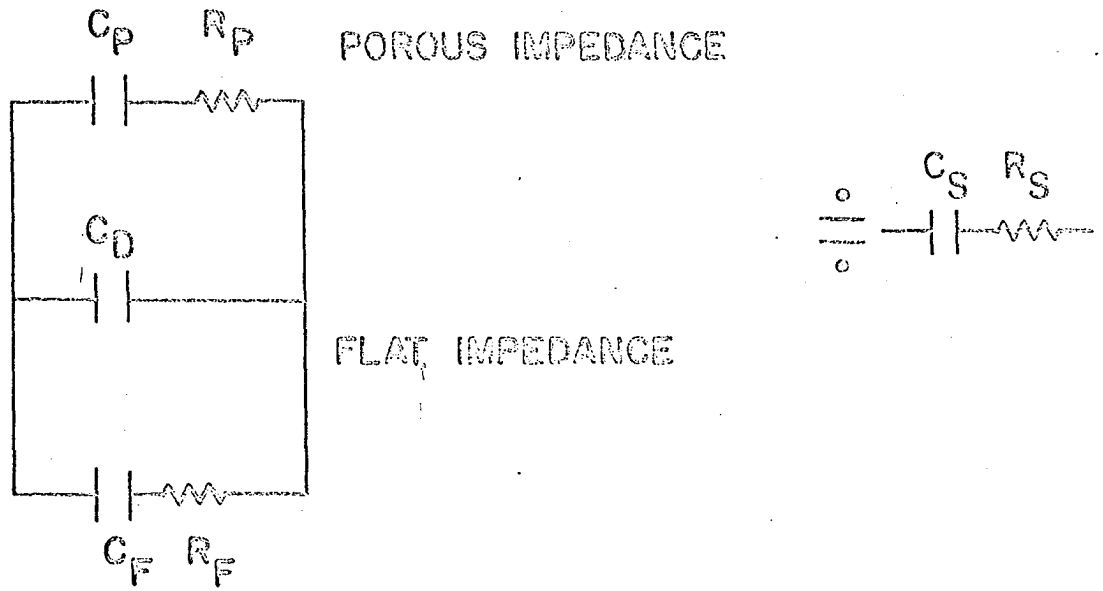

Figure 5. Circuit schematic for the AgI-solution interface

The Faradaic Impedance

The Faradaic impedance at the AgI interface is explained as follows. The potential difference between the AgI and platinum electrodes in contact via solution containing an excess of Ag^+ ions of concentration C_o in moles/cm^3 is

$$E'_C = E^{o''}_{Ag} + \frac{RT}{F} \ln C_o$$

The A.C. signal V across these electrodes changes the potential difference to E''_C such that

$$E''_C = E'_C + V$$

This means the concentration of Ag^+ ions near the AgI surface must change accordingly. Hence a concentration gradient of Ag^+ ions is set up. As a result the Ag^+ ions diffuse to and from the AgI surface according to the polarity of the signal. Let C(x,t) denote the concentration of Ag^+ ions at the distance x from the AgI surface at time t. Then

$$E''_C = E^{o''}_{Ag} + \frac{RT}{F} \ln C(o,t)$$

Using the above equations signal V is expressed as

$$V = \frac{RT}{F} \ln \frac{C(o,t)}{C_o} \qquad (9)$$

Signal V can also be expressed as

$$V = a \sin \omega t \qquad (10)$$

where a is the amplitude of the signal. Amplitude a is experimentally made small compared to a given cell potential. Under this condition

$$\frac{C_o - C(o,t)}{C_o} << 1$$

Since $$\ln \frac{C(o,t)}{C_o} = \ln \left[1 - \frac{C_o - C(o,t)}{C_o}\right]$$

then to a good approximation

$$\ln \frac{C(o,t)}{C_o} = \frac{C(o,t) - C_o}{C_o}$$

then

$$V = \frac{RT}{F} \frac{C(o,t) - C_o}{C_o} \qquad (9')$$

The diffusion of Ag^+ ions produces a current I_F called the Faradaic current. Let $Z_F = V/I_F$; then Z_F is dimensionally an impedance, and it is called the Faradaic impedance. We let the Faradaic impedance be equivalent to a series combination of a capacitance and resistance called the Faradaic capacitance and Faradaic resistance respectively.

We proceed to find an expression for the Faradaic current density I_f and subsequently expressions for the Faradaic capacitance C_F and resistance R_F resulting from planar diffusion. The Faradaic current density I_f resulting from planar diffusion in coulombs/sec cm^2 is given by

$$I_f = FDC_x(o,t) \ , \ t > 0 \qquad (11)$$

where

$$C_x(o,t) = \left[\frac{\partial C(x,t)}{\partial x}\right]_{x=0}$$

and D is the diffusion constant of Ag^+ ions in cm^2/sec. Using Fick's second law of diffusion we have

$$D\, C_{xx}(x,t) = C_t(x,t) \quad , \quad x > 0, \quad t > 0 \tag{12}$$

with the conditions

$$C(x,o) = C_o \tag{13}$$

$$\lim_{x \to \infty} C(x,t) = C_o \tag{14}$$

From Equations 9' and 10 we find

$$C(o,t) - C_o = \frac{aFC_o}{RT} \sin \omega t \tag{15}$$

It will be convenient to transform these equations as follows.

Let $U(x,t) = C(x,t) - C_o$

then Equations 11-15 become

$$I_f = F\, D\, U_x(o,t) \quad , \quad t > 0 \tag{11'}$$

$$D\, U_{xx}(x,t) = U_t(x,t) \quad , \quad x > o, \quad t > 0 \tag{12'}$$

$$U(x,o) = 0 \tag{13'}$$

$$\lim_{x \to \infty} U(x,t) = 0 \qquad (14')$$

$$U(o,t) = \frac{aFC_o}{RT} \sin \omega t \qquad (15')$$

Equations 11', 12', 14', and 15' upon Laplace Transformation yield

$$i_f = F D \bar{u}_x(o,s) \qquad (11'')$$

$$D \bar{u}_{xx}(x,s) = s \bar{u}(x,s) - U(x,o) \qquad (12'')$$

$$\lim_{x \to \infty} \bar{u}(x,s) = 0 \qquad (14'')$$

$$\bar{u}(o,s) = \frac{aFC_o}{RT} \frac{\omega}{s^2 + \omega^2} \qquad (15'')$$

Inserting Equation 13' in Equation 12'' yields

$$D \bar{u}_{xx}(x,s) - s \bar{u}(x,s) = 0$$

The solution to the above equation satisfying Equation 14'' is

$$\bar{u}(x,s) = A' \exp(-\sqrt{s/D}\, x)$$

In order to satisfy Equation 15'' we must have

$$A' = \frac{aFC_o}{RT} \frac{\omega}{s^2 + \omega^2}$$

Hence

$$u(x,s) = \frac{aFC_o}{RT} \frac{\omega}{s^2 + \omega^2} \exp(-\sqrt{s/D}\, x)$$

Differentiation of the above equation yields

$$u_x(x,s) = - \frac{aFC_o}{RT} \frac{\omega}{s^2 + \omega^2} \exp(-\sqrt{s/D}\, x)$$

then

$$u_x(o,s) = - \frac{aFC_o}{RT} \frac{\omega}{s^2 + \omega^2} \sqrt{s/D} \qquad (16)$$

Inserting Equation 16 into Equation 11'' yields

$$i_f = \frac{F^2 a\, C_o D^{1/2}}{RT} \frac{s}{s^{1/2}(s^2 + \omega^2)}$$

We now take the inverse transform of the above equation.

Let $f(s) = \frac{1}{s^{1/2}}$, $g(s) = \frac{s}{s^2 + \omega^2}$

then

$F(t) = \frac{1}{\sqrt{\pi t}}$, $G(t) = \cos\ \omega t$

$F(\tau) = \frac{1}{\sqrt{\pi \tau}}$, $G(t-\tau) = \cos\ \omega (t-\tau)$

Hence

$$I_f = \frac{F^2 a C_o D^{1/2}\, \omega}{RT} \int_o^t F(\tau)\, G(t-\tau)\, d\tau$$

$$I_f = \frac{F^2 a C_o D^{1/2}\, \omega}{RT} \int_o^t \frac{\cos\ \omega\ (t-\tau)}{\sqrt{\pi \tau}}\, d\tau$$

Since

$$\cos \omega (t - \tau) = \cos \omega t \cos \omega \tau + \sin\ \omega t \sin \omega \tau$$

then

$$I_f = \frac{F^2 a C_o D^{1/2} \omega}{RT\pi^{1/2}} \left[\cos \omega t \int_o^t \frac{\cos \omega\tau}{\sqrt{\tau}} d\tau + \sin \omega t \int_o^t \frac{\sin \omega\tau}{\sqrt{\tau}} d\tau \right]$$

Let $y = (\omega\tau)^{1/2}$

then $d\tau = \frac{2\tau^{1/2}}{\omega^{1/2}} dy$

At $\tau = 0$, $y = 0$ and at $\tau = t$, $y = \sqrt{\omega t}$

Using the above substitutions we find

$$I_f = \frac{2F^2 a C_o D^{1/2} \omega^{1/2}}{RT\pi^{1/2}} \left[\cos \omega t \int_o^{\sqrt{\omega t}} \cos y^2 dy + \sin \omega t \int_o^{\sqrt{\omega t}} \sin y^2 dy \right]$$

We consider the steady state condition where $\omega t \longrightarrow \infty$ as the upper limit in the above integrals.

Since

$$\int_o^\infty \cos y^2 dy = \frac{1}{2}\sqrt{\pi/2} = \int_o^\infty \sin y^2 dy$$

Then

$$I_f = \frac{F^2 a C_o}{RT} \left[\frac{D\omega}{2} \right]^{1/2} \left[\cos \omega t + \sin \omega t \right] \qquad (17)$$

We find another expression for the Faradaic current density I_f as follows. The Faradaic capacity C_f in farads/cm^2 and Faradaic resistivity R_f in ohm cm^2 are a series combination through which current density I_f flows. The potential drop across this combination is V. Then

$$dV = R_f dI_f + \frac{dQ_f}{C_f} \qquad (18)$$

where

$$dQ_f = I_f dt$$

We have used a differential equation above because we are considering C_f as a differential capacity. Equation 18 becomes upon use of Equation 10

$$\alpha \omega \cos \omega t = R_f \frac{dI_f}{dt} + \frac{I_f}{C_f} \tag{18'}$$

Let $Q_f = \alpha \sin \omega t + \beta \cos \omega t$

Then

$$I_f = \frac{dQ_f}{dt} = \alpha \omega \cos \omega t - \beta \omega \sin \omega t \tag{19}$$

$$\frac{dI_f}{dt} = -\alpha \omega^2 \sin \omega t - \beta \omega^2 \cos \omega t \tag{20}$$

Inserting Equations 19 and 20 in Equation 18 yields

$$\alpha \omega \cos \omega t = \left[-R_f \alpha \omega - \frac{\beta}{C_f} \right] \omega \sin \omega t + \left[-R_f \beta \omega + \frac{\alpha}{C_f} \right] \omega \cos \omega t$$

Upon equating coefficients in the above equation we get

$$\alpha = a C_f + R_f C_f \beta \omega$$

$$\beta = -R_f C_f \alpha \omega$$

Hence

$$\alpha = \frac{a C_f}{1 + (\omega C_f R_f)^2} \tag{21}$$

$$\beta = \frac{-a \omega C_f^2 R_f^2}{1 + (\omega C_f R_f)^2} \tag{22}$$

Inserting Equations 21 and 22 into Equation 19 yields

$$I_f = \frac{a\ \omega C_f}{1 + (\omega C_f R_f)^2} \left[\cos \omega t + \omega C_f R_f \sin \omega t \right] \qquad (19')$$

Upon equating coefficients of Equations 17 and 19' we get

$$\omega C_f R_f = 1$$

$$\frac{C_f}{1 + (\omega C_f R_f)^2} = \frac{F^2 C_o}{RT} \left[\frac{D}{2\omega} \right]^{1/2}$$

Hence

$$C_f = \frac{F^2 C_o}{RT} \left[\frac{2D}{\omega} \right]^{1/2} = K_f / \omega^{1/2} \qquad (23)$$

$$R_f = \frac{RT}{F^2 C_o} \left[\frac{1}{2D\omega} \right]^{1/2} = \frac{1}{K_f \omega^{1/2}} \qquad (24)$$

in which we have let

$$K_f = \frac{F^2 C_o}{RT} (2D)^{1/2} \qquad (25)$$

Let A_f denote the flat area of the AgI electrode. Then the Faradaic capacitance C_F and resistance R_F can be expressed by

$$C_F = A_f C_f \qquad (26)$$

$$R_F = R_f / A_f \qquad (27)$$

Hence

$$C_F = A_f K_f / \omega^{1/2} = K_F / \omega^{1/2} \qquad (26')$$

$$R_F = \frac{1}{A_f K_f \omega^{1/2}} = \frac{1}{K_F \omega^{1/2}} \qquad (27')$$

in which we have let

$$K_F = A_f K_f \tag{28}$$

The constant K_f for the diffusion of Ag^+ ions at 25°C is calculated from Equation 25 to be

$$K_f = 18.4\ \overline{C_o} \tag{25'}$$

where $\overline{C_o}$ is the concentration of Ag^+ ions in moles/liter. A diffusion constant of 1.20×10^{-5} cm^2/sec was used for Ag^+ ions. Hence K_F can be calculated once the value of area A_f is determined.

For the case where the solution contains an excess of I^- ions the same equations for C_F and R_F are derived.

The Pore Impedance

Using some assumptions the a.c. behavior of a pore can be represented by a uniform RC transmission line. When a small amplitude alternating voltage is used, as here, a simple derivation of the impedance of the line is possible. This has been worked out by R. De Levie (12, 13). For clarity the derivation is shown here. It is assumed that the pores are circular cylinders of uniform diameter with semi-infinite length, homogeneously filled with solution, of uniformly distributed capacitance and resistance per unit length, and without cross links. It is also assumed that any curvature of the equipotential surfaces within the pores may be neglected and that either the electrode resistance or electrolyte resistance predominates.

A diagram of a section of the uniform RC transmission line

representing the circuit of a pore is shown in Figure 5 where e(x,t) denotes the a.c. potential at distance x along the central axis of the pore at time t, i(x,t) denotes the current at distance x at time t, and $\bar{R}$ denotes the resistance of the AgI pore wall per unit pore length. In our case the electrolyte resistance is negligible compared to the AgI resistance at the ionic strengths used. Hence the electrolyte resistance has a negligible effect in the pore and is represented as the upper line in the transmission line. Impedance Z denotes the impedance of the solution - AgI interface per unit pore length. Hence Z is the impedance due to the double layer capacitance per unit pore length, $\bar{C}_D$, in parallel with the Faradaic impedance per unit pore length, $\bar{Z}_F$. The boundary conditions are

$$e(o,t) = a \sin \omega t \tag{29}$$

$$e(\infty,t) = 0 \tag{30}$$

From Figure 5 we have

$$de = - i\bar{R}dx$$

$$e = - di\ Z/dx$$

then

$$\frac{\partial e}{\partial x} + i\bar{R} = 0 \tag{31}$$

$$\frac{\partial i}{\partial x} + \frac{e}{Z} = 0 \tag{32}$$

then

$$\frac{\partial^2 e}{\partial x^2} + \bar{R}\frac{\partial i}{\partial x} = 0 \tag{33}$$

$$\frac{\partial^2 i}{\partial x^2} + \frac{1}{Z}\frac{\partial e}{\partial x} = 0 \tag{34}$$

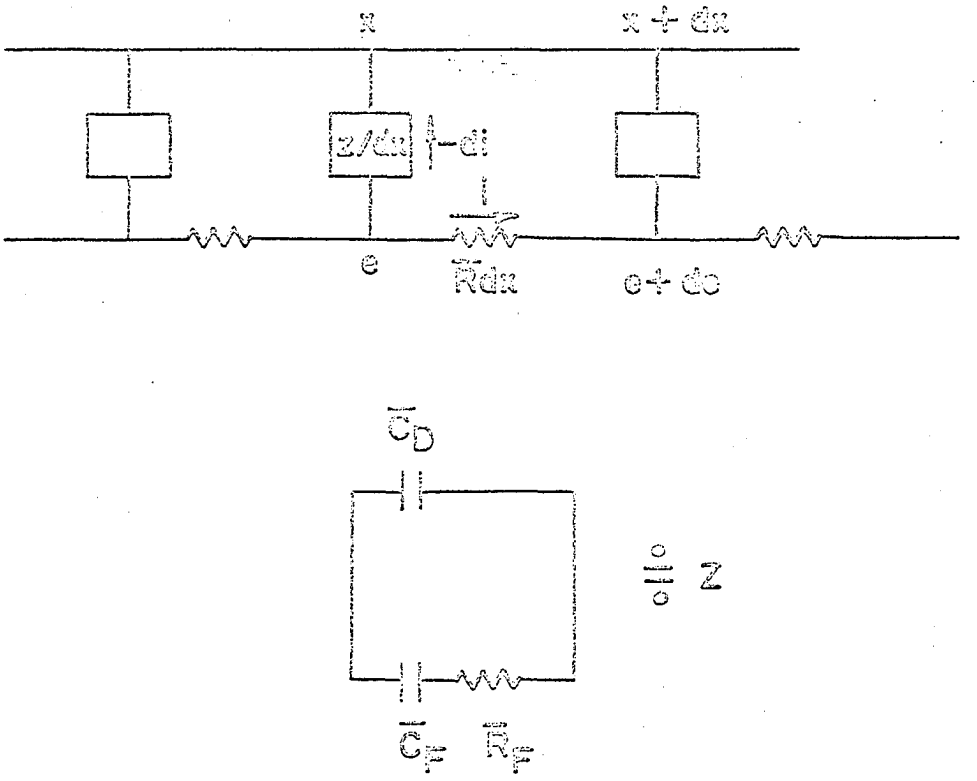

Figure 6. A section schematic of the RC transmission line for a pore

From Equations 32 and 33 we get

$$\frac{\partial^2 e}{\partial x^2} - \frac{C}{L} R = 0$$

The solution to this equation satisfying Equation 30 is

$$e(x) = A'' \exp\left(-\sqrt{R/Z}\, x\right)$$

In order to satisfy Equation 29 we must have

$$A'' = a \sin \omega t$$

Hence

$$e(x) = a \sin \omega t \exp\left(-\sqrt{R/Z}\, x\right) \qquad (35)$$

Differentiation of Equation 35 yields

$$\frac{\partial e}{\partial x} = -\sqrt{R/Z}\; a \sin \omega t \exp\left(-\sqrt{R/Z}\, x\right) \qquad (36)$$

From Equations 31 and 36 we get

$$i(x) = \frac{1}{\sqrt{RZ}}\; a \sin \omega t \exp\left(-\sqrt{R/Z}\, x\right) \qquad (37)$$

The impedance Z_A of the transmission line is

$$Z_A = \frac{e(x)}{i(x)}$$

Hence dividing Equation 35 by Equation 37 we obtain

$$Z_A = \sqrt{RZ} \qquad (38)$$

We proceed to find an expression for impedance Z. From Figure 6 we

have

$$\frac{1}{Z} = i\omega \bar{C}_D + \frac{\omega \bar{C}_f}{\omega \bar{C}_f \bar{R}_f - i} \qquad (39)$$

where $\bar{C}_f$ is the Faradaic capacitance per unit pore length in farads/cm and $\bar{R}_f$ is the Faradaic resistance per unit pore length in ohm cm. We need to find expressions for $\bar{C}_f$ and $\bar{R}_f$.

The diffusion of species i in a circular cylindrical pore is considered to be just radial. That is species i diffuses in the region $0 \leq r \leq r_o$ towards and from the electrode surface at $r = r_o$, where r is the distance from the axis of the cylinder and r_o is the radius of the pore. The Faradaic current density resulting from this diffusion is given by

$$I_f = FD\left[\frac{\partial C(r,t)}{\partial r}\right]_{r = r_o} \quad , t>0$$

where C(r,t) is the concentration of the diffusing ion at distance r at time t. According to the derivation worked out by R. De Levie (12) for the steady state condition the Faradaic current density I_f is expressed by

$$I_f = \frac{F^2 a C_o}{RT} \mu\sqrt{\omega D}\,[\sin\psi \cos \omega t + \cos\psi \sin \omega t] \qquad (40)$$

where μ and ψ are functions of λ defined by

$$\lambda = r_o\left[\frac{\omega}{D}\right]^{1/2} \qquad (41)$$

We know the Faradaic current density can also be expressed by

$$I_f = \frac{a\,\omega C_f}{1 + R_f^2 C_f^2 \omega^2} \left[\cos \omega t + \omega R_f C_f \sin \omega t\right] \qquad (19')$$

Upon equating coefficients of Equations 40 and 19' we get

$$\frac{F^2 C_o}{RT} \mu \sqrt{\omega D} \sin \psi = \frac{\omega C_f}{1 + (R_f C_f \omega)^2} \qquad (42)$$

$$\frac{F^2 C_o}{RT} \mu \sqrt{\omega D} \cos \psi = \frac{\omega C_f (\omega R_f C_f)}{1 + (R_f C_f \omega)^2} \qquad (43)$$

Dividing Equation 43 by Equation 42 yields

$$\frac{\cos \psi}{\sin \psi} = \omega R_f C_f \qquad (44)$$

From Equation 44 and 42 we get

$$C_f = \frac{F^2 C_o \mu}{RT \sin \psi} \sqrt{D/\omega} \qquad (45)$$

From Equations 44 and 45 we get

$$R_f = \frac{RT \cos \psi}{F^2 C_o \mu \sqrt{D\omega}} \qquad (46)$$

Since the pores are cylindrical with radius r_o then the area $\bar{A}_p$ of a pore of unit length is

$$\bar{A}_p = 2\pi r_o$$

Then the Faradaic capacitance per unit pore length and resistance per unit pore length can be expressed by

$$\bar{C}_F = 2\pi r_o C_f \tag{47}$$

$$\bar{R}_F = R_f / 2\pi r_o \tag{48}$$

Hence

$$\bar{C}_F = \frac{2\pi r_o F^2 C_o \mu}{RT \sin \psi} \sqrt{D/\omega} = \frac{\bar{K}_F \mu}{\sin \psi \quad \omega^{1/2}} \tag{47'}$$

$$\bar{R}_F = \frac{RT \cos \psi}{2\pi r_o F^2 C_o \mu \sqrt{D\omega}} = \frac{\cos \psi}{\bar{K}_F \mu \omega^{1/2}} \tag{48'}$$

in which we have let

$$\bar{K}_F = \frac{2\pi r_o F^2 C_o D^{1/2}}{RT} \tag{49}$$

Inserting Equations 47' and 48' into Equation 39 yields

$$\frac{1}{Z} = i \omega \bar{C}_D + \frac{\bar{K}_F \mu \sqrt{\omega}}{\cos \psi - i \sin \psi}$$

Upon rationalizing the second term we get

$$\frac{1}{Z} = \bar{K}_F \mu \sqrt{\omega} \cos \psi + i(\omega \bar{C}_D + \bar{K}_F \mu \sqrt{\omega} \sin \psi) \tag{50}$$

Hence

$$\frac{1}{\bar{R}Z} = \frac{\bar{K}_F \mu \sqrt{\omega} \cos \psi}{\bar{R}} + \frac{i}{\bar{R}} (\omega \bar{C}_D + \bar{K}_F \mu \sqrt{\omega} \sin \psi) = a + bi \tag{51}$$

in which we have let

$$a = \frac{\bar{K}_p \mu \sqrt{\omega} \cos \psi}{\bar{R}} \tag{52}$$

$$b = \frac{\omega \bar{C}_D + \bar{K}_p \mu \sqrt{\omega} \sin \psi}{\bar{R}} \tag{53}$$

Impedance Z_A can be considered equivalent to a series combination of a resistance R_A and capacitance C_A. That is

$$Z_A = R_A - \frac{i}{\omega C_A} = Z' - Z''i \tag{54}$$

We can find an expression for R_A and C_A as follows. From Equations 38, 51 and 54 we have

$$(Z' - Z''i)^2 = \frac{1}{a + bi}$$

then

$$Z'^2 - 2Z'Z''i - Z''^2 = \frac{a - bi}{a^2 + b^2}$$

Upon equating real and imaginary parts in the above equation we get

$$Z'^2 - Z''^2 = \frac{a}{a^2 + b^2} \tag{55}$$

$$Z' = \frac{b}{(a^2 + b^2)2Z''} \tag{56}$$

Using Equation 56 in Equation 55 yields

$$Z''^4 + \frac{aZ''^2}{a^2 + b^2} - \frac{b^2}{4(a^2 + b^2)} = 0$$

The solution to this equation is

$$z''^2 = \frac{(a^2 + b^2)^{1/2} - a}{2(a^2 + b^2)}$$

Then

$$-\frac{1}{\omega C_A} = z'' = \left[\frac{(a^2 + b^2)^{1/2} - a}{2(a^2 + b^2)}\right]^{1/2} \tag{57}$$

Using Equation 57 in Equation 55 yields

$$z'^2 = \frac{(a^2 + b^2)^{1/2} + a}{2(a^2 + b^2)}$$

Then

$$R_A = z' = \left[\frac{(a^2 + b^2)^{1/2} + a}{2(a^2 + b^2)}\right]^{1/2} \tag{58}$$

We can simplify the above equations in the following manner. R. De Levie (12) has tabulated ψ and μ as functions of λ. Suppose in our experimental case we have

$$\lambda = r_o \sqrt{\omega/D} \leq 1 \tag{41'}$$

Then according to the tabulation

$$\sin\psi \simeq 1 \tag{59}$$

$$\cos\psi \ll 1 \tag{60}$$

$$\mu = 1/2\lambda = 1/2\ r_o \sqrt{\omega/D} \tag{61}$$

In a qualitative sense condition 41' occurs when the radius of the pore is small compared to the length ℓ of the diffusion region in which

$$\ell \approx (D/\omega)^{1/2}$$

The diffusion constant D for Ag^+ ion is known to have a value at 25°C of

1.2×10^{-5} cm^2/sec. The angular frequency ω has an experimental maximum of 5.760×10^4 radians/sec. Hence in order for condition 41' to occur in the experimental frequency range the maximum value r_o can have is such that

$$1 = r_o\,(max)\left[\frac{5.76 \times 10^4}{1.2 \times 10^{-5}}\right]^{1/2}$$

Then

$$r_o\,(max) = 1.4 \times 10^{-5}\ cm. \qquad (41'')$$

According to our experimental data we observe that condition 41' is satisfied, as will be shown later.

By applying Equations 59 and 60 to Equations 52 and 53 we conclude that a is negligible compared to b. Hence Equations 57 and 58 reduce to

$$R_A = \left[\frac{1}{2b}\right]^{1/2} = \frac{1}{\omega C_A} \qquad (62)$$

Inserting Equation 53 with the use of Equations 59 and 61 into Equation 62 yields

$$R_A = \left[\frac{\overline{R}}{2\left[\overline{C}_D + \frac{\overline{K}_F r_o}{2D^{1/2}}\right]\omega}\right]^{1/2} = \frac{1}{\omega C_A} \qquad (62')$$

The quantity $(\overline{K}_F r_o/2D^{1/2})$ is the Faradaic capacitance per unit pore length as shown by applying Equations 59 and 61 to Equation 47'. That is

$$\overline{C}_F = \frac{\overline{K}_F r_o}{2D^{1/2}} = \frac{\pi F\ C_o r_o}{RT} \qquad (47'')$$

Hence the Faradaic impedance in the pore under condition 41' is

essentially just a capacitance independent of frequency. Note that the Faradaic resistance is negligible here. Let us express Equation 62' in terms of known quantities. We have

$$\overline{C}_D = 2\pi r_o \varkappa$$

$$\overline{R} = \frac{\rho}{2\pi r_o \tau}$$

where $\varkappa$ is the double layer capacity in farads/cm^2, ρ is the resistivity of the AgI in ohm-cm and τ is the thickness of the AgI along the pore wall. Hence Equation 62' becomes

$$R_A = \frac{1}{2\pi r_o}\left[\frac{\rho}{2\tau\left[\varkappa + \frac{F^2 C_o r_o}{2RT}\right]\omega}\right]^{1/2} \tag{63}$$

and

$$\frac{1}{C_A} = \frac{1}{2\pi r_o}\left[\frac{\rho\omega}{2\tau\left[\varkappa + \frac{F^2 C_o r_o}{2RT}\right]}\right]^{1/2} \tag{64}$$

The impedance Z_P of n_p pores is the resultant of the pore impedances connected in parallel. Assuming each pore has the same radius r_o the pore impedances are equal. Hence

$$Z_P = \frac{Z_A}{n_p}$$

Using Equations 54 and 8' we get

$$Z_p = \frac{R_A}{n_p} - \frac{i}{\omega n_p C_A} = R_p - \frac{i}{\omega C_p}$$

Equating coefficients in the above equation yields

$$C_p = n_p C_A \tag{65}$$

$$R_p = \frac{R_A}{n_p} \tag{66}$$

The surface area of n_p pores is

$$A_p = n_p \pi r_o^2 \tag{67}$$

Hence by use of Equations 63, 64, and 67 we get

$$\frac{1}{C_p} = \frac{r_o}{2A_p} \left[\frac{\rho \omega}{2\tau \left(\varkappa + \frac{F^2 C_o r_o}{2RT} \right)} \right]^{1/2} = \frac{\omega^{1/2}}{K_p} \tag{68}$$

$$R_p = \frac{r_o}{2A_p} \left[\frac{\rho}{2\tau \left(\varkappa + \frac{F^2 C_o r_o}{2RT} \right) \omega} \right]^{1/2} = \frac{1}{K_p \omega^{1/2}} \tag{69}$$

in which we have let

$$K_p = \frac{2A_p}{r_o} \left[\frac{2\tau \left(\varkappa + \frac{F^2 C_o r_o}{2RT} \right)}{\rho} \right]^{1/2} \tag{70}$$

The quantity $(F^2 C_o r_o / 2RT)$ is the Faradaic capacity C_f in the pore as shown by comparing Equations 47 and 47''. That is

$$C_f = \frac{F^2 C_o r_o}{2RT} \qquad (45')$$

Let us compare the approximate magnitudes of the double layer capacity χ and the Faradaic capacity C_f in a pore. Experimentally the Faradaic capacity is a maximum in excess Ag^+ in .1NKNO_3 at ψ = 58 millivolts where $\bar{C}_o = 3.44 \times 10^{-5}$ moles/liter. Using the maximum value for r_o from Equation 41'' at 25°C we calculate from Equation 45'

$$C_f \approx 2.6 \times 10^{-2} \bar{C}_o$$

Hence here $C_f \approx 9.0 \times 10^{-7}$ farads/cm^2. Using Agar's results as an approximation for the double layer capacity of AgI in .1N KNO_3 in this potential range we obtain

$$\chi \approx 2.8 \times 10^{-5} \text{ farads/cm}^2$$

Since χ is at least 31 times greater than C_f and the ratio becomes greater at lower positive potentials we can neglect C_f in Equations 68, 69, and 70 for positive potentials.

Experimentally the Faradaic capacity is a maximum in excess I^- in .1N KNO_3 at ψ = - 363 millivolts where $\overline{C_o} = 7.50 \times 10^{-5}$ moles/liter. Hence here

$$C_f \approx 2.0 \times 10^{-6} \text{ farads/cm}^2$$

$$\chi \approx 1.5 \times 10^{-5} \text{ farads/cm}^2$$

Since χ is at least 7.5 times greater than C_f and the ratio becomes greater at lower negative potentials we can neglect C_f in Equations 68,

69, and 70 for negative potentials.

The Impedance of the Silver Iodide-Solution Interface

We have shown that the impedance Z_S at the AgI-solution interface is

$$\frac{1}{Z_S} = \frac{\omega C_p}{\omega C_p R_p - i} + \frac{\omega C_F}{\omega C_F R_F - i} + i\,\omega C_D \qquad (68a)$$

Using Equations 26', 27', 68, and 69 we get

$$\frac{1}{Z_S} = \frac{(K_p + K_F)\sqrt{\omega} + i\,\omega\,C_D\,(1 - i)}{1 - i}$$

Let

$$K = K_p + K_F \qquad (71)$$

Then

$$Z_S = \frac{1 - i}{K\sqrt{\omega} + \omega C_D + i\,\omega\,C_D}$$

Upon rationalizing we get

$$Z_S = \frac{K/\sqrt{\omega} - i(2C_D + K/\sqrt{\omega})}{2C_D^2\,\omega + 2C_D K\,\omega^{1/2} + K^2} \qquad (72)$$

Since impedance Z_S can be represented by a series combination of resistance R_S and capacitance C_S we have

$$Z_S = R_S - i/\omega C_S \qquad (72')$$

Upon equating real and imaginary parts of Equations 72 and 72' we get

$$\frac{1}{C_S} = \frac{2C_D + K/\sqrt{\omega}}{2C_D^2 + 2C_DK/\sqrt{\omega} + K^2/\omega} \tag{73}$$

$$R_S = \frac{K/\sqrt{\omega}}{2C_D^2\omega + 2C_DK\,\omega^{1/2} + K^2} \tag{74}$$

The Impedance of Solid Silver Iodide

Solid AgI contains Frenkel defects, i.e., Ag^+ ion vacancies and Ag^+ interstitials corresponding to negative and positive charges respectively. These points defects give rise to a space charge. For a pure crystal the concentration of vacancy and interstitial defects are equal. However, in practice the crystal contains impurities. Immobile cation impurities suppress interstitial defects while immobile anion impurities suppress vacancy defects. Hence one of the defects is usually reduced to such low concentrations that it can be considered insignificant. Using the Boltzmann distribution of point defects for a crystal containing immobile cation impurities and the Poisson equation the surface charge σ_{cr} in e.s.u./cm^2 in the crystal is

$$\sigma_{cr} = \pm \left[\frac{\epsilon_c kTN_A(\infty)}{2\pi} \right]^{1/2} \left[e^{Y_c(o)} - Y_c(o) - 1 \right]^{1/2}$$

where

$$Y_c(o) = \frac{eV_c(o)}{kT}$$

in which $V_c(o)$ is the potential just inside the surface of the crystal relative to the bulk lattice, $N_A^v(\infty)$ is the number of Ag^+ ion vacancies in the bulk lattice, and ϵ_c is the dielectric constant of AgI. The

+ sign applies when $V_C(o)$ is negative and - sign when $V_C(o)$ is positive. A similar expression is found for a crystal containing immobile anion impurities. For a crystal containing completely mobile impurities the surface charge σ_{cr} is the same as for a pure crystal and is given in e.s.u./cm^2 by

$$\sigma_{cr} = \left[\frac{2 \epsilon_C kT N_A^v(\infty)}{\pi} \right]^{1/2} \sinh \frac{eV_c(o)}{2kT}$$

This is the same form as the charge density in the diffuse layer in solution. Here $N_A^v(\infty)$ will depend on the impurity content.

The capacity of the above space charge is

$$C_{cr} = \frac{d\sigma_{cr}}{dV_c(o)} \tag{75}$$

Hence for the case of immobile cation impurities we get

$$C_{cr} = \frac{e}{2kT} \left[\frac{N_A^v(\infty) \epsilon_C kT}{2\pi} \right]^{1/2} \frac{e^{Y_c(o)} - 1}{\left[e^{Y_c(o)} - Y_c(o) - 1 \right]^{1/2}}$$

For the case of immobile anion impurities we get

$$C_{cr} = \frac{e}{2kT} \left[\frac{N_A^i(\infty) \epsilon_c kT}{2\pi} \right]^{1/2} \frac{e^{-Y_c(o)} + 1}{\left[e^{-Y_c(o)} + Y_c(o) - 1 \right]^{1/2}}$$

where $N_A^i(\infty)$ is the number of Ag^+ ion interstitials in the bulk lattice. For the case of completely mobile impurities we get

$$C_{cr} = \frac{e}{2KT}\left[\frac{2\ \epsilon_c KTN_A^{v}(\infty)}{\pi}\right]^{-1/2} \cosh\frac{eV_c(o)}{2KT} \qquad (75')$$

This is the same form as the diffuse capacity in the solution.

The conductivity $1/\rho$ in $ohm^{-1}\ cm^{-1}$ in solid AgI is exclusively ionic, i.e., motion of Ag^{+} through defect positions. It is expressed by

$$1/\rho = N_A e \sum_j X_j \mu_j$$

where N_A is the number of molecules per cm^3 of the perfect crystal, X_j is the mole fraction and μ_j is the mobility in cm^2/volt-sec of the j^{th} type of defect.

We represent the impedance of the solid AgI by a series combination of a capacitance C' and resistance R'. Capacitance C' may be derived from several capacitances in series, each with a corresponding shunting resistance. For instance it could be derived from a surface capacity as described above and a bulk capacity. The shunting resistances will draw negligible current at sufficiently high frequencies. In this case they will be insignificant and C' will behave simply as the equivalent capacitance of the several capacitances in series with frequency independent capacities. We observe experimentally that this does indeed occur. This will be explained later. The resistance R', due to the ionic conductivity in solid AgI, can be expressed by

$$R' = \frac{\rho\ \tau_{eff}}{A_e} \qquad (77)$$

where τ_{eff} is the effective thickness of the AgI through which current passes. τ_{eff} is a fraction of the total AgI thickness τ_e since the

electrode is porous.

The Impedance of the Silver Iodide-Solution System

The impedance Z_S at the AgI-solution interface is in series with the impedance of solid AgI and the solution resistance R_{sol}. Then the impedance Z_V of the entire circuit is expressed by

$$Z_V = R' - \frac{i}{\omega C'} + R_S - \frac{i}{\omega C_S} + R_{sol} \tag{78}$$

Impedance Z_V consists of the series combination of the capacitance C_V and resistance R_V that make up the cell arm of the impedance bridge. That is

$$Z_V = R_V - \frac{i}{\omega C_V} \tag{78'}$$

Comparing real and imaginary parts of Equation 78 and 78' we get

$$\frac{1}{C_V} = \frac{1}{C'} + \frac{1}{C_S} \tag{79}$$

$$R_V = R_o + R_S \tag{80}$$

where

$$R_o = R' + R_{sol} \tag{81}$$

Using Equations 73 and 74 we get

$$\frac{1}{C_V} = \frac{1}{C'} + \frac{2C_D + K/\sqrt{\omega}}{2C_D^2 + 2C_D K/\sqrt{\omega} + K^2/\omega} \tag{79'}$$

$$R_V = R_o + \frac{K/\sqrt{\omega}}{2C_D^2\,\omega + 2C_D K\,\omega^{1/2} + K^2} \tag{80'}$$

A good approximation to the parameters C' and K is obtained as follows. At sufficiently low frequency C_D is small compared to $K/\sqrt{\omega}$. Hence

$$\frac{1}{C_V} \approx \frac{1}{C'} + \frac{\sqrt{\omega}}{K} \quad \text{at low frequency}$$

Thus a plot of $1/C_V$ vs $\sqrt{\omega}$ should be linear at low frequency with slope approximately 1/K and intercept approximately 1/C'. We do indeed observe such plots for frequencies at and below 1000 cps. This is illustrated in Figure 8. Since we have found that C' is independent of frequency we conclude that the shunting resistances in AgI are insignificant. Since we have found that K is independent of frequency at all potentials we conclude Equation 41' is valid. If Equation 41' were not valid the Faradaic capacitance in the pore would be significant at high potentials and frequency dependent, and hence K would contain a frequency dependent term at high potentials.

A good approximation of the parameter C_D could be obtained in principle as follows. At sufficiently high frequency C_D is large compared to $K/\sqrt{\omega}$. Hence

$$\frac{1}{C_V} \approx \frac{1}{C'} + \frac{1}{C_D} \quad \text{at very high frequency.}$$

The highest frequencies used in the present work were not sufficiently high to permit use of this approximation.

EXPERIMENTAL RESULTS

In Tables 3 - 8 are listed the experimental values of the capacitance C_V and resistance R_V for the various AgI electrodes in KNO_3 solution as function of frequency ν, potential ψ and ionic strength of the electrolyte. The corresponding calculated values based on Equations 79' and 80' are also listed along with the determined values of C_D, K, C', and R_o. All capacitance values are expressed in microfarads. All resistance values are expressed in ohms. The parameter K is expressed in farads $(\text{radians/sec})^{1/2}$. The frequency ν is expressed in cycles/sec.

The values of C_D, C', and K at a given potential were determined by finding the best fit of Equation 79' to the corresponding experimental capacitance values over the entire frequency range by use of the IBM 360/50 computer. The value of R_o at a given potential was chosen such that the experimental and calculated resistance values agreed at the highest frequency investigated. This choice was made because R_s is small there. Hence, the experimental resistance values served to check the determined values of C_V besides determining R_o. For electrode #9 we found there was considerable experimental error at the three highest frequencies at .001N solution. Hence, we did not include these data. Similarly, for electrode #10, we found considerable scatter at the two highest frequencies at .001N solution. However, the data at the lowest 5 frequencies was sufficient here to determine all the parameters, and so data for this system were included. All data at high positive potentials were also excluded.

Table 3. The experimental capacitance and resistance values at potential ψ for AgI electrode #9 in .102N KNO_3 are compared with the corresponding calculated values. The determined values of C_D, K, C' and R_o are also listed

ψ	ν	C_v		R_v		$C_D \times 10^2$	$K \times 10^5$	C'	R_o
		Exp	Calc	Exp	Calc				
32	256	1.610	1.608	400.4	400.1				
	499	1.238	1.240	315.6	315.7	16.29	8.237	7.134	142.1
	750	1.048	1.053	276.8	277.4				
	1000	.9420	.9365	254.6	254.5				
	2440	.6540	.6530	203.1	203.0				
	4944	.4933	.4970	177.6	177.6				
	9168	.3875	.3989	162.6	163.2				
6	256	1.445	1.443	419.0	414.6				
	499	1.116	1.123	325.6	324.6	14.59	7.745	5.544	138.1
	750	.9620	.9587	284.3	283.9				
	1000	.8570	.8548	259.6	259.4				
	2440	.6000	.5993	204.0	204.3				
	4944	.4579	.4566	176.9	177.0				
	9168	.3639	.3661	161.4	161.4				
-35	256	1.299	1.297	435.0	429.5				
	499	1.018	1.021	338.6	234.4	13.54	7.336	4.353	136.7
	750	.8755	.8762	291.8	291.4				
	1000	.7835	.7840	268.7	265.5				
	2440	.5530	.5541	206.4	207.2				
	4944	.4254	.4239	177.7	178.2				
	9168	.3403	.3404	161.6	161.6				
-61	256	1.232	1.233	447.9	440.4	12.89	7.129	3.938	138.2
	499	.9770	.9746	346.6	342.5				
	750	.8375	.8383	300.0	198.2				
	1000	.7500	.7511	272.6	271.5				
	2440	.5307	.5324	211.3	211.4				
	4944	.4087	.4076	181.3	181.5				
	9168	.3273	.3273	164.3	164.3				
-98	256	1.186	1.187	450.7	444.8	12.62	6.969	3.669	135.8
	499	.9440	.9413	348.3	344.7				
	750	.8105	.8111	300.9	299.4				
	1000	.7250	.7275	273.1	272.1				
	2440	.5154	.5171	210.5	210.6				
	4944	.3975	.3965	179.7	180.0				
	9168	.3189	.3188	162.4	162.4				

Table 3. Continued

ϕ	ν	C_V		R_V		$C_p \times 10^2$	$K \times 10^5$	C'	R_o
		Exp	Calc	Exp	Calc				
-137	256	1.152	1.153	452.3	448.7	12.42	6.819	3.517	133.1
	499	.9190	.9162	349.0	346.4				
	750	.7905	.7901	301.1	300.1				
	1000	.7080	.7090	272.8	272.2				
	2440	.5034	.5047	209.0	209.4				
	4944	.3878	.3874	177.8	178.1				
	9168	.3117	.3117	160.2	160.2				
-181	256	1.1880	1.120	458.6	453.6	12.32	6.723	3.308	133.8
	499	.8950	.8923	354.3	349.9				
	750	.7710	.7708	305.7	302.9				
	1000	.6920	.6926	277.1	274.6				
	2440	.4935	.4945	212.1	211.0				
	4944	.3803	.3804	180.4	179.3				
	9168	.3066	.3065	161.2	161.2				
-209	256	1.114	1.116	459.2	454.2	12.43	6.705	3.293	134.1
	499	.8930	.8897	353.9	350.2				
	750	.7690	.7687	305.0	303.1				
	1000	.6900	.6903	276.1	274.7				
	2440	.4928	.4936	211.7	211.0				
	4944	.3801	.3800	179.8	179.4				
	9168	.3063	.3064	161.3	161.3				
-240	256	1.107	1.108	459.2	454.4	12.48	6.720	3.214	135.1
	499	.8880	.8852	352.3	350.7				
	750	.7660	.7656	305.4	303.7				
	1000	.6870	.6884	276.8	275.4				
	2440	.4920	.4928	211.9	211.9				
	4944	.3800	.3797	180.1	180.3				
	9168	.3063	.3065	162.2	162.2				
-278	256	1.113	1.114	455.9	451.3	12.63	6.733	3.249	133.1
	499	.8920	.8894	350.6	347.8				
	750	.7690	.7690	301.8	300.9				
	1000	.6900	.6915	273.2	272.7				
	2440	.4943	.4949	208.9	209.4				
	4944	.3818	.3815	177.6	177.9				
	9168	.3080	.3081	159.9	159.9				

Table 3. Continued

ψ	ν	C_V		R_V		$C_D \times 10^2$	$K \times 10^5$	C'	R_o
		Exp	Calc.	Exp	Calc				
-296	256	1.123	1.124	464.6	456.2	12.80	6.756	3.313	139.4
	499	.8990	.8964	357.2	353.0				
	750	.7750	.7748	308.3	306.3				
	1000	.6930	.6964	279.4	278.2				
	2440	.4971	.4482	215.1	215.2				
	4944	.3842	.3841	183.7	183.9				
	9168	.3105	.3104	166.0	166.0				
-331	256	1.175	1.175	463.2	455.6	13.10	6.659	3.922	135.2
	499	.9280	.9265	354.8	351.1				
	750	.7960	.7960	305.2	303.9				
	1000	.7120	.7129	276.2	275.4				
	2440	.5047	.5038	211.3	211.7				
	4944	.3893	.3887	180.0	180.3				
	9168	.3138	.3138	162.4	162.4				
-363	256	1.298	1.299	466.6	460.6	13.36	6.539	6.108	137.3
	499	1.000	.9980	357.6	354.4				
	750	.8460	.8465	307.6	306.3				
	1000	.7520	.7521	278.2	277.4				
	2440	.5225	.5239	212.7	213.9				
	4944	.4001	.3991	181.0	181.1				
	9168	.3204	.3208	163.2	163.2				

It is observed that the calculated and experimental values of C_V and R_V agree very well, usually within 1 percent.

The value of R_o should be independent of potential at a given ionic strength. The slight variation that is observed may be due to a variation in the geometry of the cell.

Representative plots of C_V vs $\frac{1}{\omega^{1/2}}$ are shown in Figure 7 for electrode #9 at .1N. Representative plots of $\frac{1}{C_V}$ vs $\omega^{1/2}$ are shown in Figure 8 for electrode #9 at .1N.

Table 4. The experimental capacitance and resistance values at potential ψ for AgI electrode #10 in .102N KNO_3 are compared with the corresponding calculated values. The determined values of C_D, K, C', and R_o are also listed

ψ	ν	C_ν		R_ν		$C_D \times 10^2$	$K \times 10^5$	C'	R_o
		Exp	Calc	Exp	Calc				
58	256	1.6010	1.5990	361.9	353.9	25.00	9.577	4.666	142.8
	499	1.2780	1.2810	281.8	282.1				
	750	1.1120	1.1130	248.1	249.9				
	1000	1.0060	1.0050	229.0	230.6				
	2440	.7400	.7345	188.2	188.3				
	4944	.5753	.5807	168.1	168.1				
	9168	.4601	.4625	156.4	157.1				
32	256	1.3110	1.3070	381.4	372.0	22.13	8.868	3.122	142.0
	499	1.0620	1.0720	298.1	294.3				
	750	.9430	.9421	260.0	259.4				
	1000	.8600	.8571	238.1	238.5				
	2440	.6420	.6373	191.9	192.4				
	4944	.5083	.5080	170.2	170.2				
	9168	.4148	.4236	158.1	158.1				
6	256	1.1460	1.1460	405.6	383.0	20.76	8.459	2.462	140.0
	499	.9520	.9563	307.0	301.4				
	750	.8430	.8445	265.7	264.7				
	1000	.7720	.7723	242.5	242.8				
	2440	.5857	.5817	193.4	194.3				
	4944	.4704	.4669	171.0	171.0				
	9168	.3863	.3909	158.2	158.2				
-35	256	1.0180	1.0168	419.0	393.1	20.00	8.085	2.014	140.4
	499	.8540	.8557	314.3	307.9				
	750	.7610	.7635	270.3	269.5				
	1000	.7000	.7015	246.3	246.6				
	2440	.5385	.5363	195.0	195.9				
	4944	.4365	.4332	171.5	171.6				
	9168	.3608	.3648	158.2	158.2				
-36	256	.8730	.9690	425.9	403.8	18.72	7.663	1.932	139.2
	499	.8120	.8160	318.5	413.0				
	750	.7250	.7281	273.6	273.7				
	1000	.6650	.6692	248.3	249.6				
	2440	.5157	.5114	195.4	196.5				
	4944	.4183	.4150	171.1	171.1				
	9168	.3463	.3505	157.3	157.3				

Table 4. Continued

ψ	ν	C_y		K_y		$C_p \times 10^2$	$K \times 10^5$	C'	R_o
		Exp	Calc	Exp	Calc				
-98	256	.9230	.9198	432.6	412.3	19.11	7.420	1.798	139.1
	499	.7740	.7770	322.3	319.6				
	750	.6920	.6945	278.6	277.9				
	1000	.6370	.6391	251.2	253.1				
	2440	.4945	.4901	197.2	198.2				
	4944	.4014	.3985	172.2	172.1				
	9168	.3331	.3371	157.8	157.8				
-137	256	.8880	.8850	437.8	415.5	18.87	7.363	1.682	139.9
	499	.7480	.7510	325.8	322.0				
	750	.6700	.6732	279.2	280.0				
	1000	.6200	.6205	253.2	255.0				
	2440	.4829	.4700	198.6	199.6				
	4944	.3920	.3898	173.2	173.2				
	9168	.3259	.3302	158.9	158.9				
-181	256	.8550	.8529	445.2	422.6	18.69	7.219	1.596	142.1
	499	.7230	.7258	330.9	327.4				
	750	.6495	.6516	283.5	284.5				
	1000	.6010	.6014	257.0	259.0				
	2440	.4696	.4649	201.4	202.7				
	4944	.3824	.3800	175.7	175.8				
	9168	.3183	.3226	161.2	161.2				
-209	256	.8490	.8472	446.1	423.6	18.65	7.206	1.578	142.6
	499	.7190	.7215	331.4	328.2				
	750	.6460	.6480	283.8	285.3				
	1000	.5980	.5982	257.5	259.7				
	2440	.4675	.4628	202.0	203.3				
	4944	.3809	.3785	176.4	176.4				
	9168	.3170	.3214	161.8	161.8				
-240	256	.8390	.8376	449.8	424.9	18.69	7.191	1.548	143.5
	499	.7120	.7144	333.6	329.3				
	750	.6400	.6422	285.6	286.3				
	1000	.5932	.5932	258.9	260.7				
	2440	.4646	.4597	203.3	204.2				
	4944	.3789	.3764	177.3	177.3				
	9168	.3157	.3200	162.7	162.7				

Table 4. Continued

ψ	ν	C_V		R_V		$C_D \times 10^2$	$K \times 10^5$	C'	R_o
		Exp	Calc	Exp	Calc				
-278	256	.8520	.8492	451.5	425.2	18.85	7.152	1.595	143.1
	499	.7190	.7223	383.9	329.2				
	750	.6460	.6484	285.2	286.0				
	1000	.5980	.5984	260.6	260.3				
	2440	.4670	.4618	202.4	203.6				
	4944	.3812	.3787	176.8	176.7				
	9168	.3177	.3219	162.1	162.1				
-296	256	.8545	.8517	451.6	424.8	18.88	7.146	1.605	142.6
	499	.7210	.7241	383.2	328.7				
	750	.6470	.6493	284.5	285.5				
	1000	.5991	.5996	257.7	259.8				
	2440	.4682	.4636	201.8	203.1				
	4944	.3818	.3792	176.2	176.2				
	9168	.3180	.3223	161.6	161.6				
-331	256	.8930	.8890	465.7	438.7	19.21	6.852	1.814	143.1
	499	.7430	.7468	388.9	333.8				
	750	.6620	.6659	288.3	289.0				
	1000	.6010	.6119	260.4	262.4				
	2440	.4741	.4687	202.7	204.0				
	4944	.3850	.3822	176.6	176.5				
	9168	.3206	.3248	161.8	161.8				
-363	256	.9970	.9939	472.3	446.4	19.19	6.483	2.492	143.0
	499	.8080	.8125	345.1	341.2				
	750	.7120	.7139	292.6	293.1				
	1000	.6490	.6499	263.6	266.2				
	2440	.4930	.4866	203.7	205.2				
	4944	.3943	.3925	176.8	176.8				
	9168	.3271	.3318	161.7	161.7				

Table 5. The experimental capacitance and resistance values at potential ψ for AgI electrode #9 in .0102N KNO_3 are compared with the corresponding calculated values. The determined values of C_D, K, C', and R_o are also listed

ψ	ν	C_V		R_V		$C_D \times 10^2$	$K \times 10^5$	C'	R_o
		Exp	Calc	Exp	Calc				
3	256	1.0320	1.0340	1486	1487	8.009	4.983	5.937	1048
	499	.7880	.7933	1340	1347				
	750	.6580	.6588	1202	1203				
	1000	.5800	.5818	1141	1245				
	2440	.3963	.3968	1154	1158				
	4944	.2974	.2962	1112	1114				
	9168	.2311	.2330	1088	1088				
-11	256	1.0010	1.0020	1496	1498	8.145	4.905	5.359	1049
	499	.7650	.7624	1353	1351				
	750	.6410	.6427	1285	1286				
	1000	.5665	.5684	1245	1247				
	2440	.3894	.3894	1157	1159				
	4944	.2933	.2916	1113	1115				
	9168	.2289	.2302	1089	1089				
-25	256	.9850	.9840	1508	1507	8.600	4.770	5.459	1055
	499	.7480	.7478	1360	1361				
	750	.6280	.6303	1292	1294				
	1000	.5562	.5575	1251	1254				
	2440	.3837	.3829	1162	1165				
	4944	.2903	.2880	1119	1120				
	9168	.2268	.2286	1094	1094				
-47	256	.9520	.9498	1516	1515	9.057	4.639	5.062	1055
	499	.7220	.7240	1363	1364				
	750	.6095	.6115	1294	1296				
	1000	.5402	.5418	1252	1255				
	2440	.3757	.3743	1162	1164				
	4944	.2859	.2833	1119	1119				
	9168	.2247	.2265	1093	1093				
-69	256	.9310	.9294	1514	1517				
	499	.7100	.7105	1362	1365	9.142	4.588	4.727	1054
	750	.5984	.6010	1294	1296				
	1000	.5312	.5330	1253	1255				
	2440	.3709	.3694	1159	1163				
	4944	.2631	.2804	1115	1017				
	9168	.2227	.2246	1092	1092				

Table 5. Continued

ψ	ν	Cv		Ry		$C_p \times 10^2$	$K \times 10^5$	C'	R_o
		Exp	Calc	Exp	Calc				
-98	256	.9040	.9025	1515	1519				
	499	.6920	.6930	1362	1366	9.009	4.542	4.259	1051
	750	.5859	.5875	1293	1296				
	1000	.5204	.5218	1252	1255				
	2440	.3638	.3628	1159	1161				
	4944	.2778	.2757	1113	1115				
	9168	.2195	.2211	1089	1089				
-127	256	.8890	.8876	1513	1515				
	499	.6830	.6839	1359	1361	8.460	4.534	3.973	1046
	750	.5793	.5808	1288	1292				
	1000	.5153	.5163	1247	1250				
	2440	.3606	.3598	1153	1157				
	4944	.2760	.2738	1108	1110				
	9168	.2179	.2197	1084	1084				
-184	256	.8700	.8690	1521	1525				
	499	.6710	.6715	1367	1371	8.808	4.487	3.727	1052
	750	.5695	.5710	1296	1300				
	1000	.5073	.5080	1255	1258				
	2440	.3553	.3546	1161	1164				
	4944	.2718	.2700	1116	1117				
	9168	.2152	.2167	1091	1091				
-213	256	.8650	.8643	1516	1521				
	499	.6680	.6680	1362	1365	8.946	4.468	3.715	1046
	750	.5669	.5682	1290	1295				
	1000	.5052	.5056	1248	1252				
	2440	.3543	.3534	1153	1158				
	4944	.2714	.2695	1109	1111				
	9168	.2147	.2166	1084	1084				
-264	256	.8600	.8596	1514	1518				
	499	.6655	.6654	1389	1363	9.108	4.470	3.615	1045
	750	.5653	.5664	1287	1292				
	1000	.5046	.5044	1246	1250				
	2440	.3546	.3533	1152	1156				
	4944	.2718	.2699	1107	1109				
	9168	.2154	.2174	1083	1083				

Table 5. Continued

ψ	ν	C_V		R_V		$C_D \times 10^2$	$K \times 10^5$	C'	R_o
		Exp	Calc	Exp	Calc				
-288	256	.8650	.8640	1517	1517				
	499	.6685	.6690	1362	1362	9.211	4.497	3.624	1047
	750	.5684	.5696	1290	1293				
	1000	.5064	.5074	1248	1251				
	2440	.3564	.3555	1154	1157				
	4944	.2737	.2718	1109	1111				
	9168	.2174	.2190	1085	1085				
-321	256	.8810	.8808	1516	1519	9.569	4.465	4.026	1049
	499	.6785	.6785	1361	1363				
	750	.5755	.5764	1289	1293				
	1000	.5129	.5127	1247	1251				
	2440	.3599	.3587	1153	1157				
	4944	.2755	.2744	1109	1111				
	9168	.2199	.2216	1085	1085				
-345	256	.9110	.9104	1523	1524				
	499	.6830	.6937	1364	1366	10.15	4.372	5.144	1051
	750	.5865	.5864	1291	1295				
	1000	.5198	.5203	1249	1252				
	2440	.3642	.3626	1155	1157				
	4944	.2797	.2779	1110	1111				
	9168	.2230	.2253	1086	1086				

Table 6. The experimental capacitance and resistance values at potential ψ for AgI electrode #10 in .0102N KNO_3 are compared with the corresponding calculated values. The determined values of C_D, K, C', and R_o are also listed

ψ	ν	C_V		R_V		$C_D \times 10^2$	$K \times 10^2$	C'	R_o
		Exp	Calc	Exp	Calc				
38	256	1.0280	1.0280	1434	1415	13.42	5.870	3.340	1062
	499	.8150	.8138	1304	1397				
	750	.7010	.7015	1247	1244				
	1000	.6290	.6299	1215	1212				
	2440	.4514	.4519	1142	1142				
	4944	.3414	.3516	1111	1107				
	9168	.2677	.2877	1089	1088				
3	256	.8550	.8534	1462	1449	12.57	5.106	2.506	1048
	750	.5900	.5926	1249	1253				
	1000	.5343	.5345	1211	1216				
	2440	.3937	.3836	1133	1136				
	4944	.3095	.3056	1096	1097				
	9168	.2464	.2525	1076	1076				
-11	256	.8350	.8224	1468	1454	12.75	5.065	2.286	1052
	499	.6585	.6625	1310	1318				
	750	.5750	.5766	1253	1257				
	1000	.5209	.5214	1215	1220				
	2440	.3865	.3813	1136	1140				
	4944	.3049	.3015	1100	1101				
	9168	.2444	.2501	1080	1080				
-25	256	.7990	.7958	1474	1459	13.06	4.996	2.136	1054
	499	.6400	.6439	1320	1321				
	750	.5591	.5620	1253	1259				
	1000	.5004	.5092	1216	1222				
	2440	.3799	.3749	1137	1141				
	4944	.3018	.2978	1100	1102				
	9168	.2427	.2482	1081	1081				
-47	256	.7680	.7659	1472	1459	13.29	4.951	1.958	1053
	499	.6200	.6256	1319	1320				
	750	.5438	.5462	1251	1258				
	1000	.4959	.4960	1214	1221				
	2440	.3745	.3678	1134	1140				
	4944	.2962	.2937	1099	1101				
	9168	.2407	.2458	1080	1080				

Table 6. Continued

ψ	ν	C_V		R_V		$C_D \times 10^2$	$K \times 10^5$	C'	R_c
		Exp	Calc	Exp	Calc				
-39	256	.7500	.7476	1477	1480	13.44	4.940	1.847	1054
	499	.6080	.6113	1321	1321				
	750	.5342	.5368	1253	1259				
	1000	.4880	.4883	1216	1222				
	2440	.3694	.3689	1138	1140				
	4944	.2949	.2915	1100	1101				
	9168	.2393	.2446	1081	1081				
-98	256	.7230	.7200	1478	1468	13.31	4.903	1.705	1054
	499	.5889	.5919	1323	1323				
	750	.5180	.5213	1254	1260				
	1000	.4742	.4750	1218	1223				
	2440	.3602	.3557	1136	1141				
	4944	.2890	.2857	1100	1102				
	9168	.2354	.2402	1081	1081				
-127	256	.7070	.7043	1480	1465	13.27	4.857	1.639	1053
	499	.5775	.5804	1324	1324				
	750	.5089	.5118	1254	1261				
	1000	.4666	.4689	1216	1223				
	2440	.3545	.3505	1135	1140				
	4944	.2855	.2821	1099	1101				
	9168	.2327	.2375	1080	1080				
-184	256	.6830	.6808	1487	1470	13.12	4.834	1.526	1055
	499	.5611	.5608	1330	1328				
	750	.4930	.4985	1260	1264				
	1000	.4551	.4555	1221	1226				
	2440	.3478	.3434	1138	1143				
	4994	.2805	.2770	1101	1104				
	9168	.2285	.2335	1082	1082				
-213	256	.6760	.6738	1489	1470	13.08	4.800	1.504	1053
	499	.5557	.5584	1328	1327				
	750	.4918	.4940	1258	1263				
	1000	.4511	.4515	1219	1225				
	2440	.3452	.3407	1137	1141				
	4994	.2752	.2750	1100	1102				
	9168	.2268	.2319	1080	1080				

Table 6. Continued

ψ	ν	C_V		R_V		$C_D \times 10^2$	$K \times 10^5$	C'	R_o
		Exp	Calc	Exp	Calc				
-284	256	.6690	.6[illegible]9	1493	1476	13.17	4.767	1.482	1057
	499	.5506	.5531	1332	1332				
	750	.4875	.4896	1263	1268				
	1000	.4470	.4477	1223	1220				
	2440	.3429	.3384	1142	1145				
	4944	.2769	.2736	1105	1103				
	9168	.2259	.2310	1084	1084				
-288	256	.6710	.6686	1497	1475	13.31	4.799	1.478	1059
	499	.5518	.5550	1333	1332				
	750	.4892	.4915	1264	1260				
	1000	.4491	.4496	1225	1220				
	2440	.3447	.3401	1142	1148				
	4944	.27[illegible]3	.2752	1103	1107				
	9168	.2275	.2325	1086	1086				
-321	256	.6820	.6792	1500	1475	13.55	4.756	1.547	1058
	499	.5536	.5618	1335	1331				
	750	.4940	.4966	1265	1267				
	1000	.4529	.4533	1224	1229				
	2440	.3475	.3427	1141	1145				
	4844	.2830	.2772	1105	1106				
	9168	.2292	.2345	1085	1085				
-351	256	.7100	.7074	1516	1486	14.24	4.568	1.794	1061
	499	.5745	.5701	1341	1338				
	750	.5053	.5030	1267	1271				
	1000	.4626	.4627	1226	1232				
	2440	.3523	.3475	1143	1146				
	4944	.2850	.2814	1106	1105				
	9168	.2331	.2390	1086	1086				

Table 7. The experimental capacitance and resistance values at potential ψ for AgI electrode #11 in .0102N KNO_3 are compared with the corresponding calculated values. The determined values of C_β, K, C', and R_o are also listed.

ψ	ν	C_ν		R_ν		$C_\beta \times 10^2$	$K \times 10^3$	C'	R_o
		Exp	Calc	Exp	Calc				
-9	256	.9760	.9783	1413	1406	14.13	7.188	2.119	1111
	499	.8100	.8095	1312	1310				
	750	.7160	.7148	1267	1266				
	1000	.6510	.6517	1241	1240				
	2440	.4843	.4843	1180	1181				
	4944	.3836	.3826	1151	1152				
	9168	.3130	.3146	1135	1135				
-31	256	.9290	.9282	1409	1407	14.90	7.066	1.935	1109
	499	.7740	.7742	1306	1308				
	750	.6860	.6864	1259	1264				
	1000	.6260	.6276	1234	1237				
	2440	.4715	.4706	1174	1178				
	4944	.3758	.3745	1147	1149				
	9168	.3090	.3102	1132	1132				
-54	256	.8900	.8900	1415	1411	15.18	7.037	1.755	1114
	499	.7480	.7477	1311	1313				
	750	.6650	.6656	1265	1260				
	1000	.6100	.6104	1238	1242				
	2440	.4622	.4614	1179	1182				
	4944	.3703	.3694	1152	1153				
	9168	.3058	.3072	1137	1137				
-77	256	.8550	.8542	1420	1414	15.40	7.102	1.631	1119
	499	.7230	.7230	1316	1316				
	750	.6450	.6464	1271	1272				
	1000	.5940	.5944	1244	1246				
	2440	.4542	.4551	1185	1187				
	4944	.3658	.3647	1157	1158				
	9168	.3031	.3045	1142	1142				
-108	256	.8290	.8286	1420	1414	15.69	7.183	1.525	1123
	499	.7060	.7057	1318	1318				
	750	.6330	.6334	1273	1274				
	1000	.5832	.5840	1247	1248				
	2440	.4488	.4484	1188	1190				
	4944	.3638	.3626	1160	1161				
	9168	.3027	.3039	1145	1145				

Table 7. Continued

ψ	ν	C_V		R_V		$C_3 \times 10^2$	$K_3 \times 10^7$	C'	R_3
		Exp	Calc	Exp	Calc				
-152	256	.8000	.8006	1418	1417	15.59	7.199	1.430	1126
	499	.6860	.6855	1319	1321				
	750	.6170	.6171	1275	1277				
	1000	.5701	.5702	1249	1251				
	2440	.4408	.4402	1192	1193				
	4944	.3578	.3571	1164	1164				
	9168	.2988	.2999	1148	1148				
-203	256	.7830	.7836	1428	1423	15.96	7.219	1.374	1134
	499	.6730	.6734	1329	1327				
	750	.6080	.6076	1284	1284				
	1000	.5676	.5624	1258	1258				
	2440	.4376	.4364	1201	1200				
	4944	.3560	.3554	1172	1172				
	9168	.2982	.2995	1156	1156				
-244	256	.7725	.7729	1435	1430	16.16	7.252	1.386	1143
	499	.6660	.6660	1336	1335				
	750	.6020	.6019	1292	1292				
	1000	.5560	.5577	1264	1266				
	2440	.4353	.4342	1207	1208				
	4944	.3555	.3545	1179	1180				
	9168	.2977	.2993	1165	1165				
-272	256	.7725	.7726	1426	1421	16.30	7.274	1.383	1135
	499	.6660	.6661	1327	1326				
	750	.6030	.6022	1284	1283				
	1000	.5576	.5581	1257	1257				
	2440	.4363	.4349	1200	1200				
	4944	.3564	.3554	1173	1172				
	9168	.2986	.3002	1157	1157				
-308	256	.7775	.7775	1428	1418	16.59	7.304	1.343	1134
	499	.6700	.6702	1326	1324				
	750	.6050	.6060	1281	1281				
	1000	.5619	.5616	1254	1255				
	2440	.4390	.4378	1198	1198				
	4944	.3593	.3580	1170	1171				
	9168	.3010	.3027	1155	1155				

Table 8. The experimental capacitance and resistance values at potential ψ for AgI electrode #10 in .00102N KNO_3 are compared with the corresponding calculated values. The determined values of C_D, K, C', and R_o are also listed

ψ	ν	C_V		R_V		$C_D \times 10^2$	$K \times 10^5$	C'	R_o
		Exp	Calc	Exp	Calc				
-1	256	.7030	.7010	8140	8148	5.587	3.153	6.025	7463
	499	.5220	.5228	7922	7927				
	750	.4340	.4366	7820	7826				
	1000	.3820	.3840	7763	7766				
	2440	.2605	.2600	7630	7630				
	4944	.1775	.1939	7571	7562				
	9168	.1105	.1531	7537	7523				
-25	256	.6360	.6348	8140	8151	6.232	2.964	4.186	7441
	499	.4800	.4794	7914	7917				
	750	.4010	.4032	7800	7811				
	1000	.3540	.3564	7744	7747				
	2440	.2460	.2455	7606	7606				
	4944	.1730	.1861	7546	7536				
	9168	.1100	.1493	7510	7497				
-64	256	.5890	.5861	8140	8120	7.138	2.925	2.801	7420
	499	.4490	.4512	7888	7885				
	750	.3800	.3835	7773	7778				
	1000	.3410	.3415	7715	7715				
	2440	.2410	.2406	7575	7575				
	4944	.1710	.1858	7516	7507				
	9168	.1100	.1517	7480	7470				
-72	256	.5820	.5784	8140	8122	7.301	2.943	2.575	7428
	499	.4440	.4474	7875	7888				
	750	.3770	.3813	7767	7782				
	1000	.3410	.3401	7707	7719				
	2440	.2410	.2407	7580	7580				
	4944	.1710	.1865	7522	7513				
	9168	.1100	.1527	7484	7477				
-105	256	.5560	.5540	8140	8102	7.566	2.925	2.182	7410
	499	.4300	.4325	7874	7867				
	750	.3690	.3705	7758	7762				
	1000	.3320	.3316	7691	7699				
	2440	.2370	.2369	7560	7560				
	4944	.1695	.1849	7502	7493				
	9168	.1100	.1523	7470	7457				

Table 8. Continued

ψ	ν	C_V		R_V		$C_{Dp} \times 10^2$	$K \times 10^5$	C'	R_o
		Exp	Calc	Exp	Calc				
-126	256	.5500	.5482	8105	8087	7.806	2.956	2.037	7381
	499	.4280	.4300	7833	7834				
	750	.3670	.3691	7725	7730				
	1000	.3320	.3308	7665	7667				
	2440	.2370	.2371	7529	7529				
	4944	.1700	.1853	7470	7464				
	9168	.1100	.1528	7440	7428				
-186	256	.5350	.5336	8085	8089	7.961	2.913	1.903	7372
	499	.4190	.4202	7829	7824				
	750	.3600	.3617	7713	7716				
	1000	.3250	.3249	7648	7656				
	2440	.2350	.2345	7517	7517				
	4944	.1700	.1846	7464	7452				
	9168	.1105	.1532	7433	7417				
-221	256	.5290	.5277	8105	8085	8.244	2.876	1.887	7396
	499	.4150	.4160	7846	7847				
	750	.3570	.3584	7730	7741				
	1000	.3220	.3222	7665	7676				
	2440	.2340	.2335	7539	7539				
	4944	.1700	.1846	7477	7474				
	9168	.1105	.1539	7444	7440				
-251	256	.5260	.5248	8140	8106	8.288	2.887	1.826	7420
	499	.4120	.4143	7873	7869				
	750	.3560	.3574	7750	7763				
	1000	.3220	.3215	7691	7700				
	2440	.2340	.2334	7562	7562				
	4944	.1700	.1847	7496	7498				
	9168	.1105	.1541	7469	7463				
-286	256	.5200	.5261	8150	8126	8.611	2.869	1.870	7443
	499	.4140	.4154	7885	7889				
	750	.3560	.3584	7770	7783				
	1000	.3220	.3225	7705	7720				
	2440	.2360	.2347	7582	7582				
	4944	.1720	.1864	7521	7519				
	9168	.1115	.1561	7488	7485				
-322	256	.5370	.5346	8110	8071	8.744	2.864	1.986	7389
	499	.4190	.4208	7843	7833				
	750	.3600	.3625	7731	7727				
	1000	.3250	.3259	7663	7664				
	2440	.2380	.2369	7527	7527				
	4944	.1725	.1882	7466	7464				
	9168	.1120	.1577	7433	7430				

Figure 7. Dependence of series equivalent capacitance on frequency at various potentials (millivolts relative to zero point of charge) for AgI-aqueous KNO_3 system

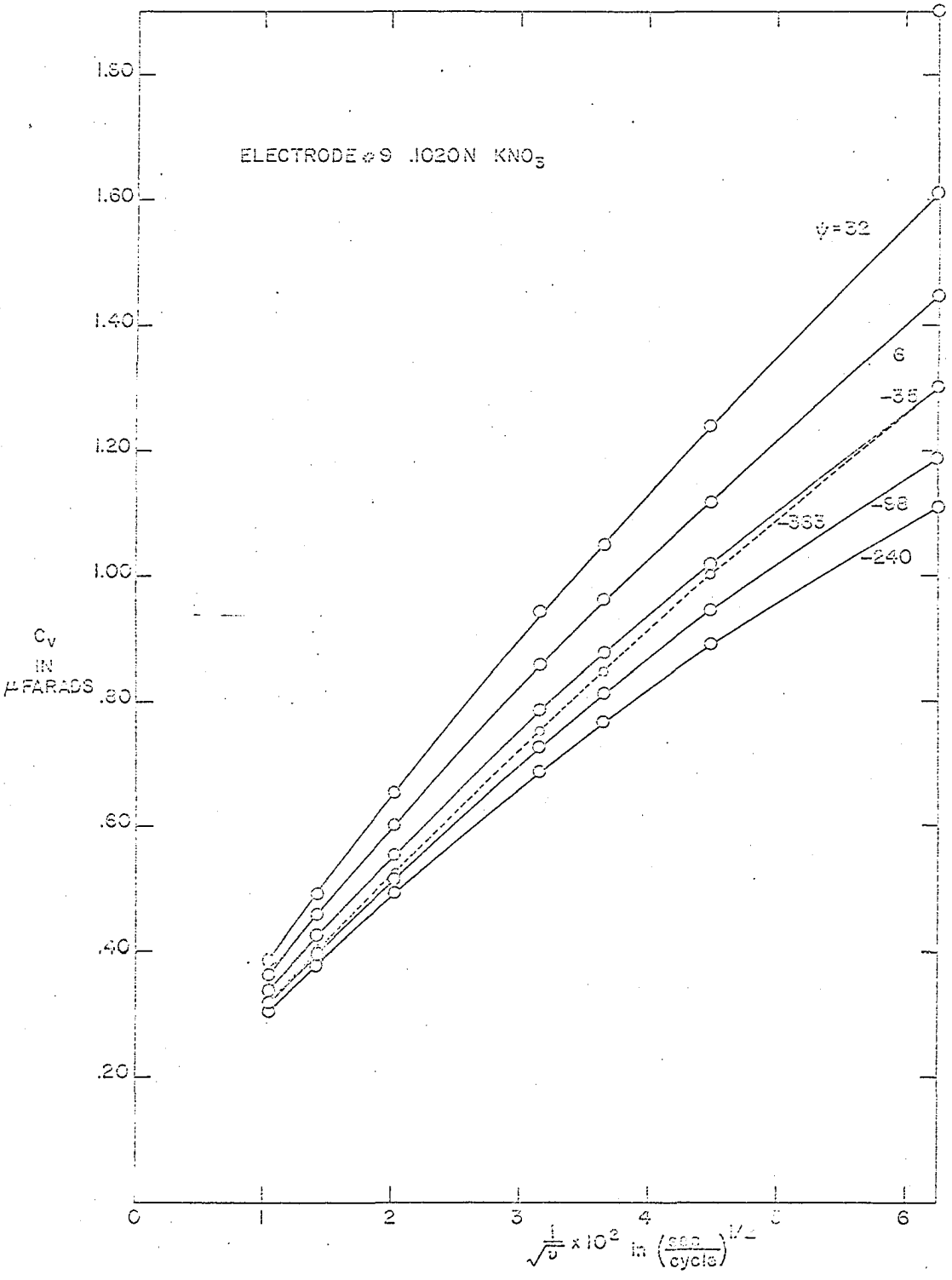
ELECTRODE #9 .1020N KNO3
ψ=32
6
-35
-88
-333
-240
1.80
1.60
1.40
1.20
1.00
.80
.60
.40
.20
0
1
2
3
4
5
6
Cv IN μFARADS
1/√υ x 10² in (sec/cycle)^1/2

Figure 8. Dependence of reciprocal series equivalent capacitance on frequency at various potentials (millivolts relative to zero point of charge) for AgI-aqueous KNO_3 system

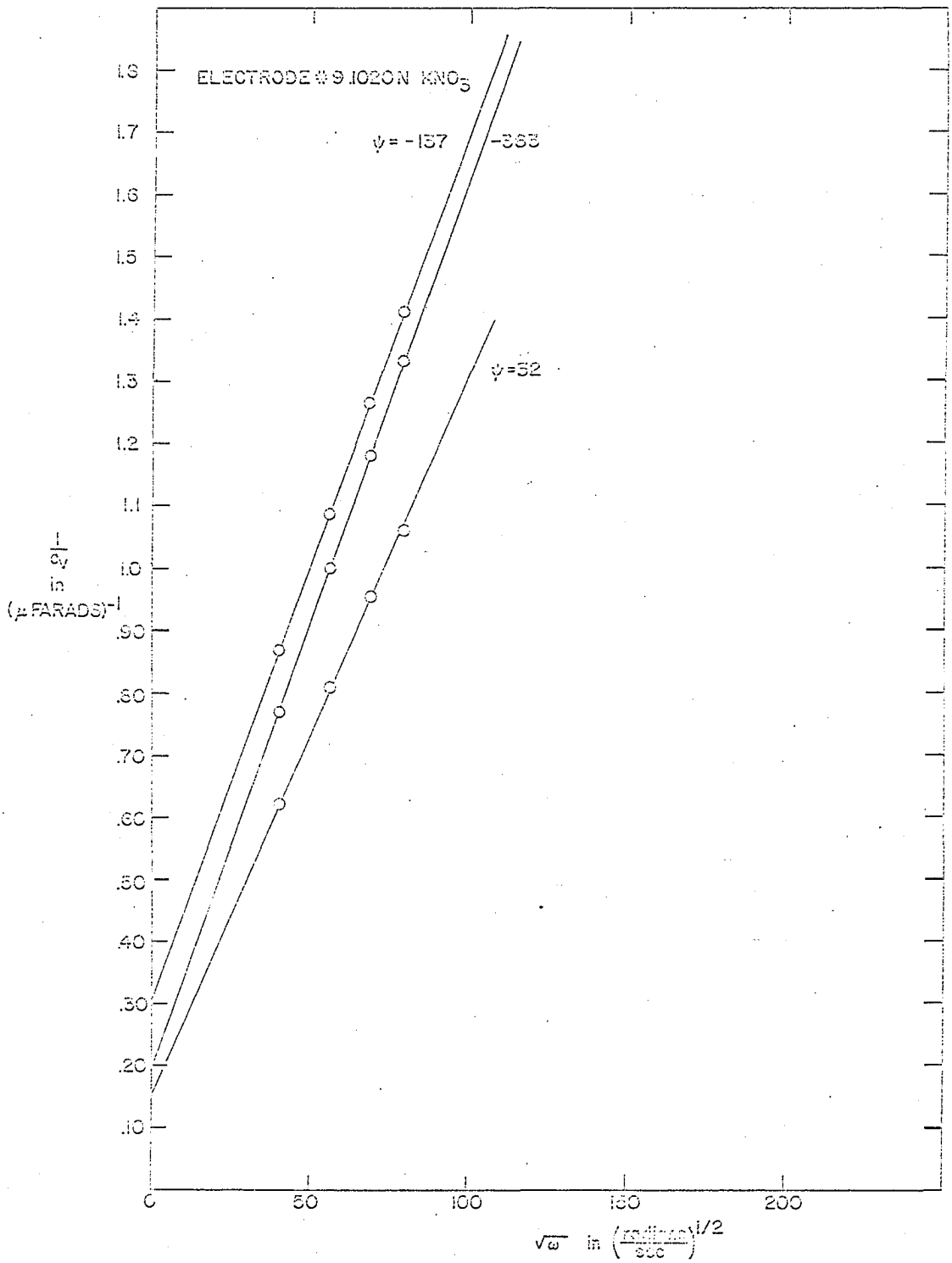
ELECTRODE #9 .102ON KNO3
ψ = -157
-383
ψ=-52
1.8
1.7
1.6
1.5
1.4
1.3
1.2
1.1
1.0
.90
.80
.70
.60
.50
.40
.30
.20
.10
0
50
100
150
200
1/cV in (μ FARADS)-1
√ω in (radians/sec)1/2

DISCUSSION

The area A_f of the flat, smooth portion of the AgI electrode is determined by assuming the value of the AgI double layer capacity κ at the zero point of charge in .001N KNO_3 solution to be equal to that for the Hg-NaF solution interface under the same conditions. The latter value is 6.00 μfarads/cm^2 at 25°C according to the reliable work of D. C. Grahame (2). This is a very reasonable assumption since the double layer capacity is very nearly equal to the surface independent diffuse capacity under the above conditions as discussed previously.

Since

$$A_f = C_D/\kappa \qquad (82)$$

then A_f can be calculated from the value of C_D measured under these conditions. This method is appropriate for electrode #10 in which double layer capacitance C_D values can be determined in .001N solution. For electrodes #9 and #11 area A_f is determined from the value of the AgI double layer capacity of electrode #10 near $\psi = 0$ in .01N solution. The values of area A_f in cm^2 for the various electrodes are listed in Table 9.

The area A_p of the porous portion of the AgI electrode is calculated by using the relation

$$A_p = A_e - A_f$$

The values of area A_p in cm^2 for the various electrodes are listed in Table 9. A comparison of the values of A_p and A_f for a given electrode shows that the electrode surface is largely porous.

Table 9. The values of the total area A_g, the flat area A_f, and the porous area A_p of the various electrodes in cm^2

Electrode	$A_g \times 10^2$	$A_f \times 10^2$	$A_p \times 10^2$	$A_p^2/A_f \times 10^2$
# 9	3.58	.593	2.99	15.1
#10	3.57	.931	2.64	7.48
#11	2.64	1.045	1.60	2.45

The Silver Iodide Double Layer Capacity

The values of the AgI double layer capacity χ at a given potential ψ and ionic strength of KNO_3 can be calculated once A_f is determined. Such values of χ for the various electrodes are listed in Tables 10-12. Plots of χ vs ψ at a given ionic strength of KNO_3 for the various electrodes are shown in Figures 9-11. The χ values at a given potential ψ and ionic strength for the 3 electrodes agree within 10 percent for negative potentials and within 15 percent for positive potentials.

Since there is no minimum at and near the zero point of charge in the χ - ψ plot at .1N solution than the AgI double layer capacity approximately equals the Stern capacity here. The sharp rise in χ for positive potentials at .1N solution is mainly attributed to the specific adsorption of NO_3^- ions. The small rise in χ at high negative potentials ($|\psi| \geq 200$ mv.) may be due to the specific adsorption of K^+ ions. This rise is also observed in .01N KNO_3 solution. On the other hand it may be largely due to a decreasing thickness of the Stern layer

resulting from the compression of the solvent molecules by the high electrical field emanating from the surface which is believed to cause the increase also observed in the double layer capacity at the Hg-solution interface at high negative potentials.

At high potentials the double layer capacity approximately equals the Stern capacity unless specific adsorption occurs. Since the Stern capacity is independent of the electrolyte concentration then the double layer capacity χ values at the various electrolyte concentrations should tend to converge at high negative potentials. However, no such convergence is observed at high negative potentials. This non-convergence of χ indicates that specific adsorption of K^+ ions occurs in this potential range. An observation of the double layer capacity values for the Hg-NaF solution interface based on Grahame's work show that values of χ at .1N and .01N electrolyte concentrations converge at high negative potentials while the χ values at .001N fall somewhat below this convergence.

The surface charge density σ_o at a given potential ψ can be obtained by integration of the χ - ψ curve provided that $d\psi \approx d\psi_o$.

Since $$d\sigma_o = \chi d\psi_o \qquad (1')$$

then by assuming $$d\psi = d\psi_o \qquad (83)$$

$$\sigma_o = \int_o^{\psi} \chi d\psi$$

The conditions under which Equation 83 is valid are found as follows. Let φ denote the AgI half cell potential. That is

$$\varphi = E_c - E_{cal} \qquad (84)$$

Potential φ can be expressed by

$$\phi = V_c(o) + \chi + \psi_o \qquad (84')$$

where χ denotes the surface potential jump due to the dipole orientation of the solvent.

Since $$\psi = E_c - E_c(zpc) \qquad (7)$$

then from Equations 84 and 84'

$$\psi = \phi - \phi\,(zpc)$$

$$\psi = \psi_o + V_c(o) - V_c(o)(zpc) + \chi - \chi\,(zpc) \qquad (7'')$$

Hence if the variations of $V_c(o)$ and χ with surface charge σ_o are very small compared to those of ψ_o or if the change of $V_c(o)$ is compensated by an approximately equal but opposite change of χ then

$$d\psi \approx d\psi_o$$

Experimental values of χ and $V_c(o)$ have not been obtainable. Hence the validity of Equation 83 cannot be checked directly. Though we have not integrated the $\chi - \psi$ curve it would be useful to do. In the potential region where no specific adsorption occurs and by assuming that Equation 83 is valid in that potential region this integration yields the diffuse charge density σ_g. Then the potential at the outer Helmholtz plane ψ_δ can be calculated and hence the diffuse capacity can likewise be calculated. The Stern capacity could then be determined by use of Equation 1. If the Stern capacity thus obtained proved to be independent of electrolyte concentration this would indicate that both of the above assumptions are valid, if not, that one or both are invalid. Since we have already indicated that specific adsorption is likely at positive potentials and

at high negative potentials then this integration would yield only the surface charge density σ_o in these potential regions provided Equation 83 is valid. We will compare our results with those of other workers and arrive at possible conclusions relative to these assumptions in this way.

Most recently Lyklema and Overbeek (8) and Agar (10) have studied the AgI-solution interface by measuring the adsorption of the potential determining ions on a AgI surface using a titration method. By differentiation of the surface charge-potential ψ curve they purport to obtain the differential capacitance C_D of the AgI double layer. It was assumed that $d\psi \sim d\psi_o$, otherwise the differentiation would not yield C_D correctly. By setting the value of the double layer capacity $\varkappa$ at the zero point of charge in .001N solution of indifferent electrolyte equal to that for the Hg-NaF solution double layer under the same conditions they obtain the surface area of the AgI and hence $\varkappa$ at any other potential ψ and ionic strength.

Plots of the differential capacity $\varkappa$ of the AgI-KNO_3 solution double layer vs potential ψ at various ionic strengths of KNO_3 as determined by Agar are shown in Figure 12. Lyklema's plots of $\varkappa$ vs ψ at various ionic strengths of KNO_3 agree within 10 percent with those of Agar's except at high negative potentials where Lyklema's values decrease markedly while Agar's values decrease only slightly. This is in contrast to our observed rise in $\varkappa$ at high negative potentials. A rise in the double layer capacity at the Ag_2S-solution interface at high negative potentials has been observed by Iwasaki and DeBruyn (14). However, unlike our case their values do converge at the various ionic

Table 10. The AgI double layer capacity $\varkappa$ in microfarads/cm^2 and the AgI resistivity ρ, expressed as ρ/α' in ohms are listed for electrode #9 at a given potential ψ in millivolts and ionic strength of KNO_3

.102N KNO_3			.0102N KNO_3		
ψ	$\varkappa$	ρ/α'	ψ	$\varkappa$	ρ/α'
32	27.5	24.8	3	13.5	32.8
6	24.6	24.6	-11	13.7	34.2
-35	22.8	25.2	-25	14.5	38.0
-61	21.7	25.4	-47	15.3	42.2
-98	21.3	26.0	-69	15.4	43.5
-137	20.95	26.7	-98	15.2	43.7
-181	20.8	27.3	-127	15.1	43.6
-209	20.95	27.7	-184	14.85	43.6
-240	21.05	27.7	-213	15.1	44.9
-278	21.3	28.1	-264	15.55	45.8
-296	21.6	28.5	-288	15.5	46.2
-331	22.1	31.7	-321	16.1	50.5
-363	22.5	40.8	-351	17.1	63.1

Table 11. The AgI double layer capacity $\varkappa$ in microfarads/cm^2 and the AgI resistivity ρ, expressed as ρ/α' in ohms are listed for electrode #10 at a given potential ψ in millivolts and ionic strength of KNO_3

.102N KNO_3			.0102N KNO_3			.00102N KNO_3		
ψ	$\varkappa$	ρ/α'	ψ	$\varkappa$	ρ/α'	ψ	$\varkappa$	ρ/α'
58	26.85	30.9	38	14.4	42.8	-1	6.00	58.4
32	23.8	29.6	3	13.5	49.5	-25	6.69	72.1
6	22.3	29.6	-11	13.7	50.5	-64	7.67	83.7
-35	21.5	30.7	-25	14.0	52.8	-72	7.84	84.5
-61	21.2	33.6	-47	14.3	54.4	-105	8.13	88.5
-98	20.5	34.7	-69	14.4	55.2	-126	8.17	87.0
-137	20.3	34.8	-98	14.3	55.4	-186	8.55	93.9
-181	20.1	35.9	-127	14.25	56.25	-221	8.85	99.9
-209	20.05	35.9	-184	14.1	56.2	-251	8.90	100.2
-240	20.1	36.2	-213	14.05	56.85	-286	0.25	107.7
-278	20.25	37.3	-264	14.15	58.4	-322	9.42	120.4
-296	20.3	38.0	-288	14.3	59.0			
-331	20.6	45.7	-321	14.55	64.6			
-363	20.6	70.9	-351	15.3	88.7			

Table 12. The AgI double layer capacity $\varkappa$ in microfarads/cm^2 and the AgI resistivity ρ, expressed as ρ/α' in ohm cm^2 liquid for electrode #11 at a given potential ψ in millivolts in .0100N KNO_3

ψ	$\varkappa$	ρ/α'
-9	13.7	28.1
-31	14.25	30.0
-54	14.5	30.45
-77	14.75	30.55
-108	15.0	30.4
-152	14.9	30.1
-203	15.3	30.65
-244	15.45	30.85
-272	15.6	31.2
-308	15.9	32.65

strengths employed at a high negative potential but then overlap. Our $\varkappa$ values agree very well with those of Agar around the zero point of charge.

The increasing difference between our and Agar's or Lyklema's $\varkappa$ values at high negative potentials indicate that Equation 83 is not valid, i.e. $d\psi$ and $d\psi_o$ are not approximately equal, in this region and hence the differentiation of the σ - ψ plot would not yield the double layer capacity $\varkappa$. Thus Agar's or Lyklema's values would be incorrect in this potential range and so would differ from our results which do not depend on the validity of Equation 83. The indicated invalidity of Equation 83 at high negative potentials means that the variation in potential $V_c(c)$

Figure 9. Dependence of differential double layer capacity on potential (relative to potential at zero point of charge) and supporting electrolyte concentration for the AgI-KNO_3 solution interface

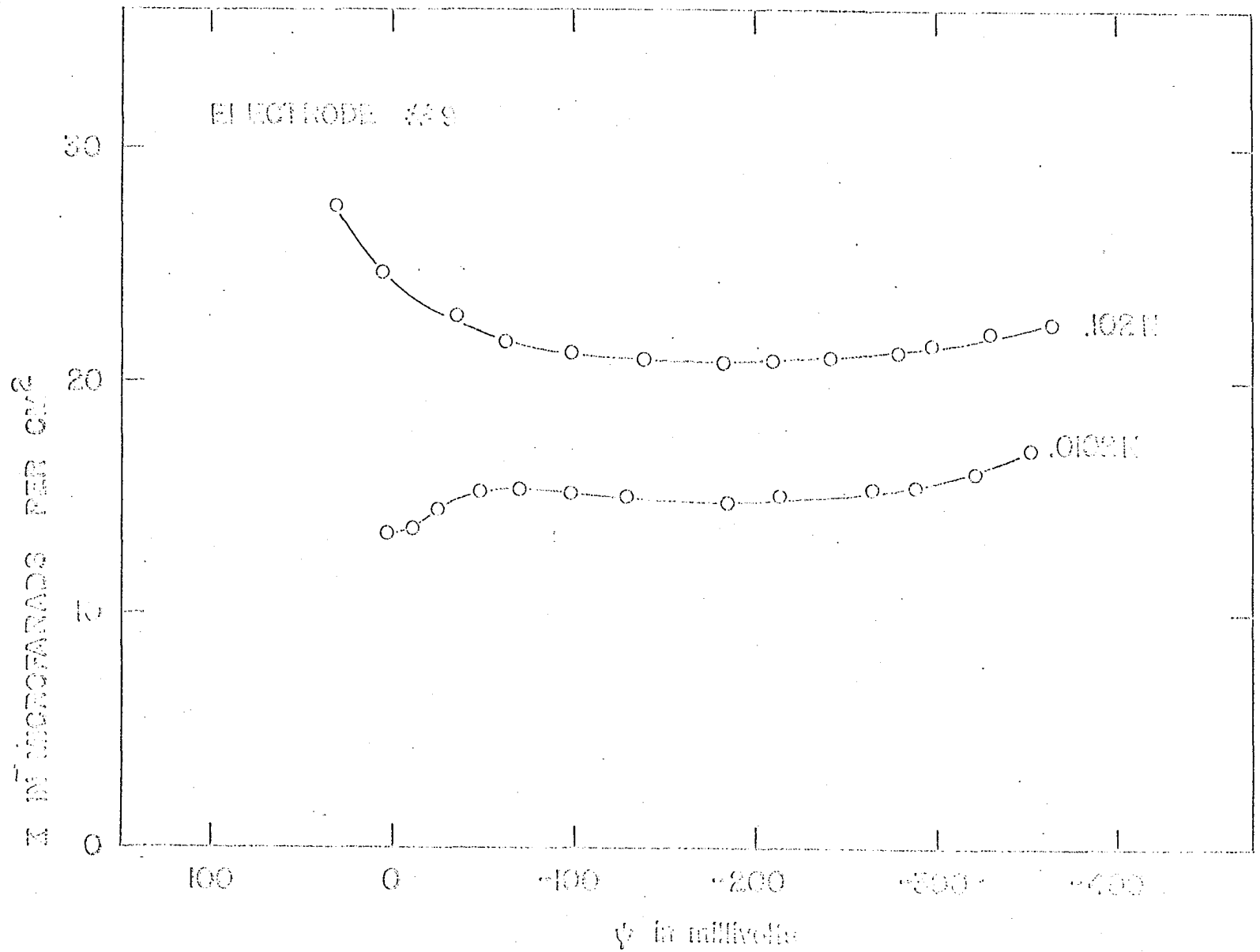
ELECTRODE: #9
30
20
10
0
100
0
-100
-200
-300
-400
ψ in millivolts

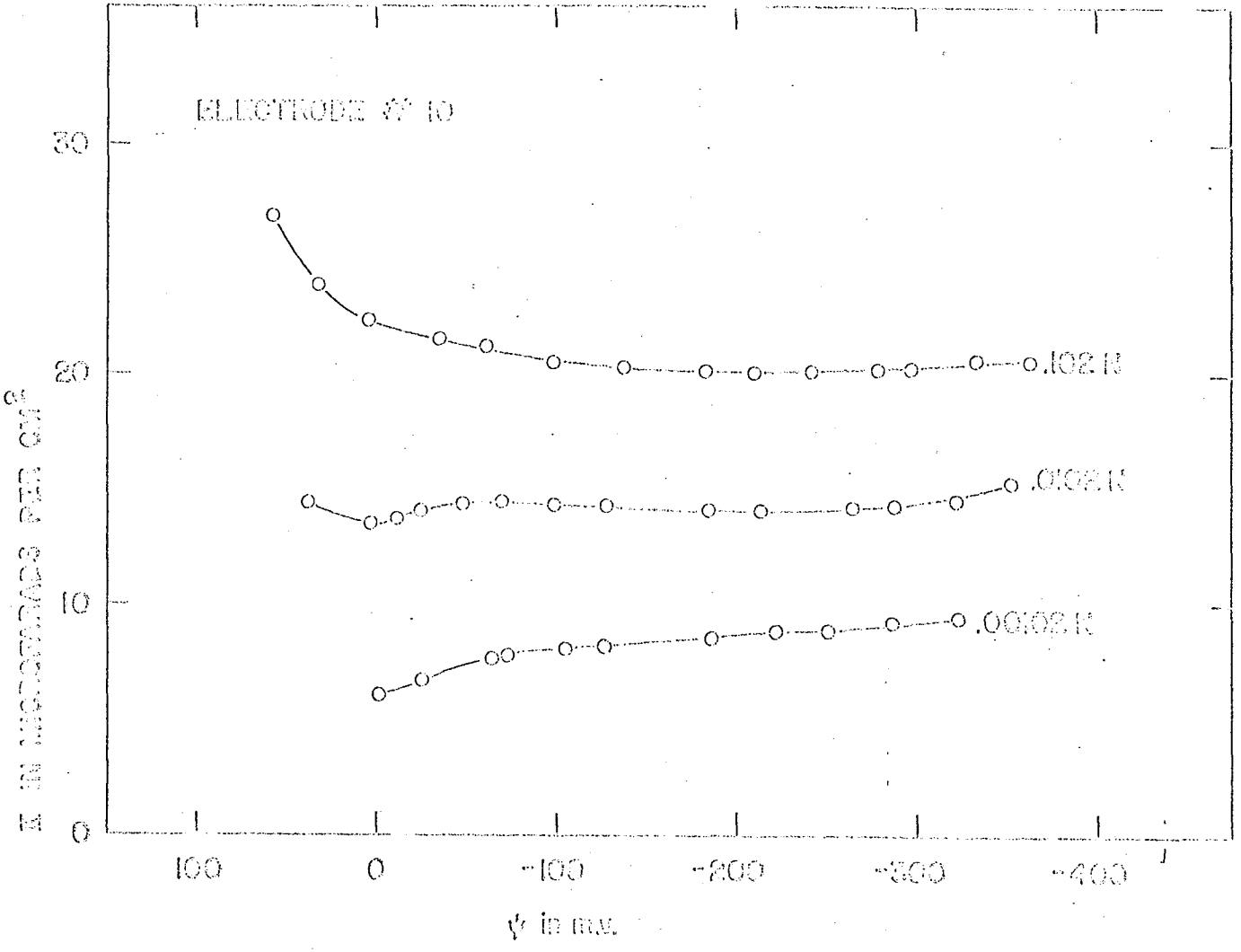

Figure 10. Dependence of differential double layer capacity on potential (relative to potential at zero point of charge) at supporting electrolyte concentration for the $AgI-KNO_3$ solution interface

Figure 11. Dependence of differential double layer capacity on potential (relative to potential at zero point of charge) at supporting electrolyte concentration of .01M for the AgI-KNO_3 solution interface

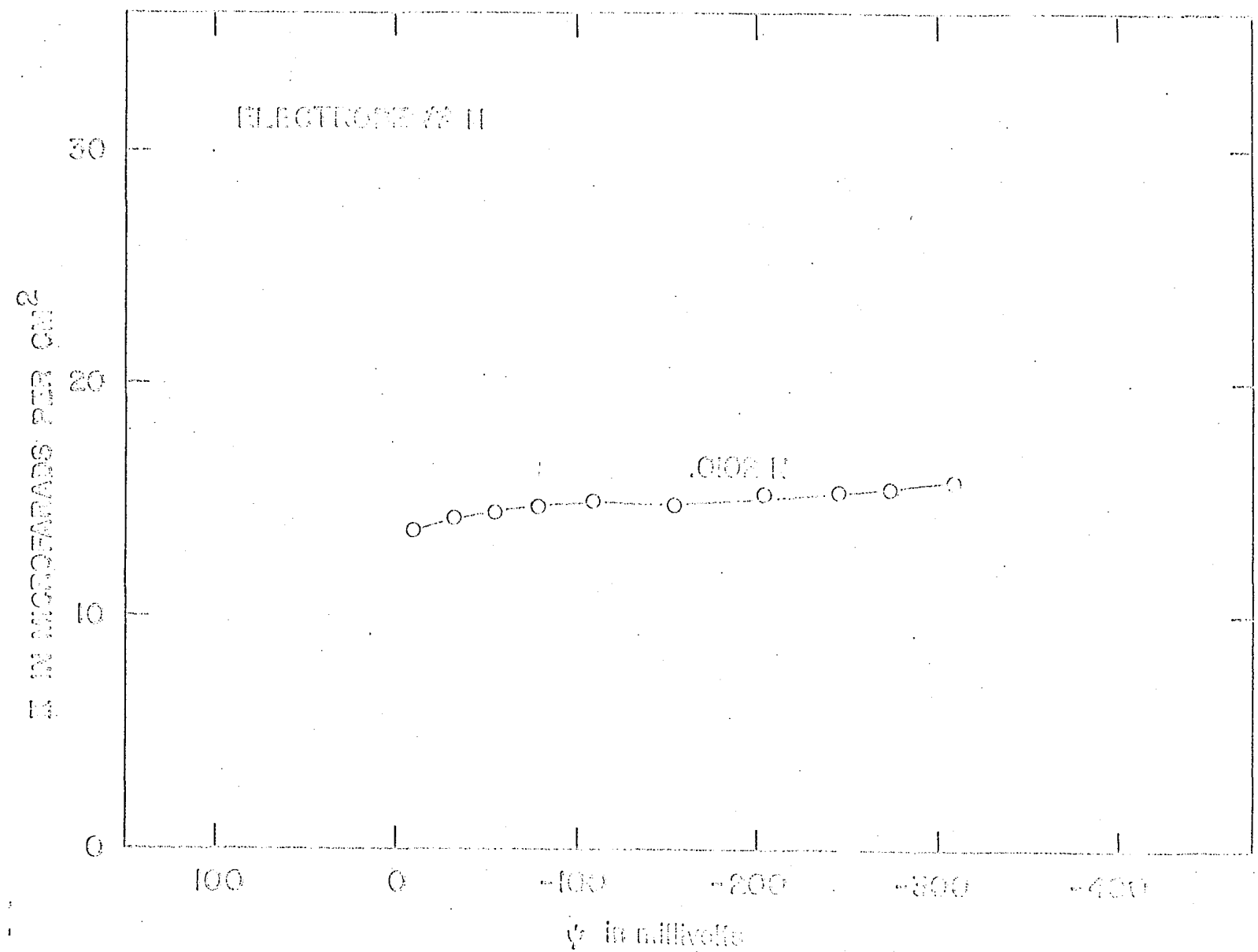
ELECTRODE # 11
30
20
10
0
100
0
-100
-200
-300
-400
ψ in millivolts

Figure 12. Dependence of differential double layer capacity on potential (relative to potential at zero point of charge) and supporting electrolyte concentration for the AgI-KNO_3 solution interface

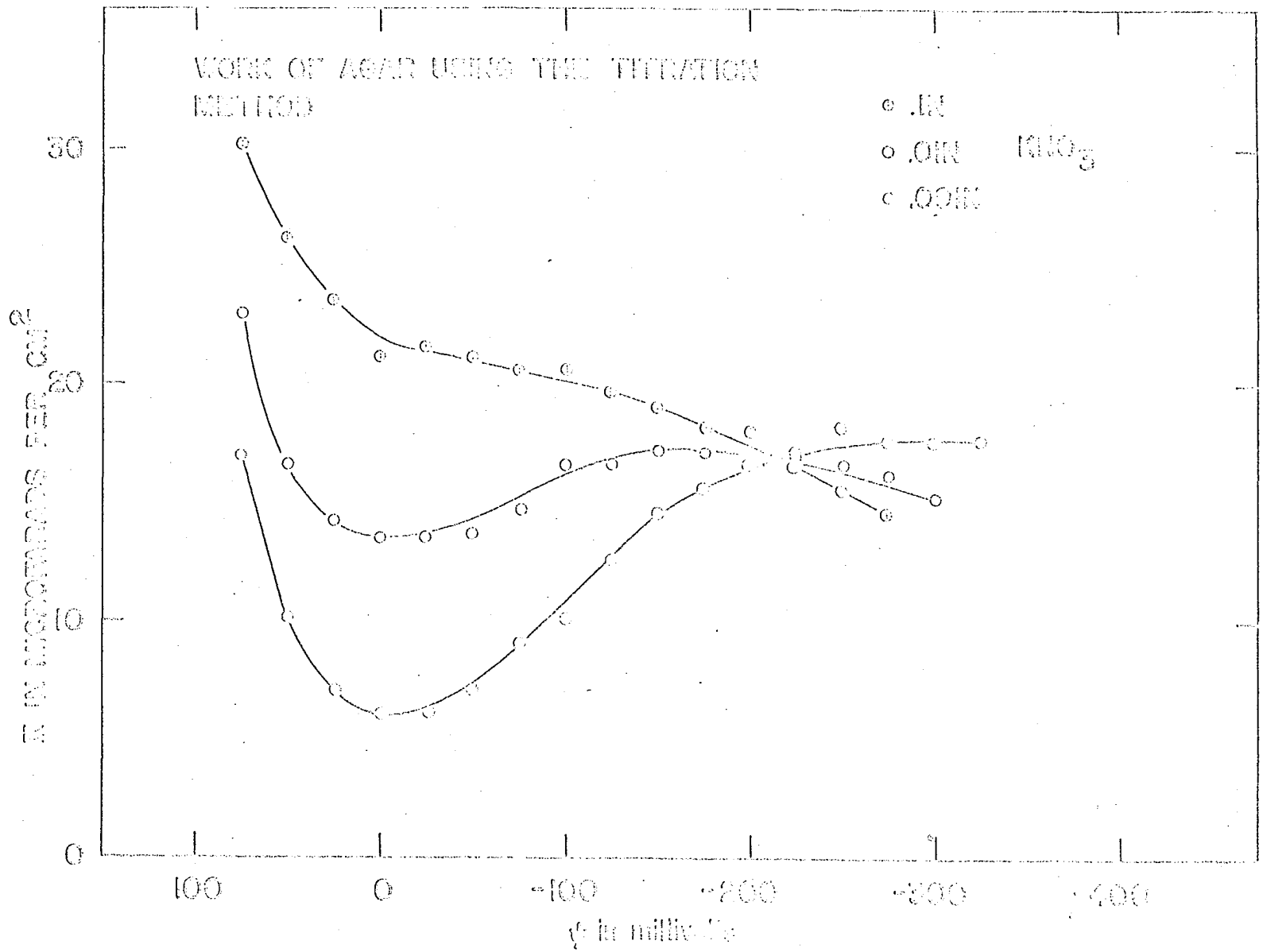
WORK OF AGAR USING THE TITRATION METHOD
.1N
.01N
.001N
$KMnO_4$
30
20
10
0
100
0
-100
-200
-300
-400
in millivolts

and or potential χ is significant in this potential region. It should be noted that both Lyklema's and Agar's experimental results become increasingly more inaccurate at high negative potentials. In fact there is overlap of the $\pi - \phi$ curves at the various electrolyte concentrations in this potential region. This inaccuracy also contributed to the difference between their observed values π values and ours at high negative potentials.

The good agreement between Agar's π values and ours around the zero point of charge (small potentials) indicates that Equation 68 is valid in this potential region. In the discussion of capacitance C' of solid AgI it will be indicated that the variation of potential $V_c(o)$ around the zero point of charge is significant. Hence in order for $d\phi \approx d\psi_o$ around the zero point of charge the changes of potential χ must be approximately equal but opposite to the above change of $V_c(o)$ around the zero point of charge.

The Resistivity of Silver Iodide

The resistivity ρ of AgI can be estimated from the experimental parameters. In the experimental potential range we have

$$K_p = \left[\frac{2A_p}{r_o} \quad \frac{2\tau}{\rho} \pi \right]^{1/2} \tag{70}$$

Using Equation 62 we get

$$\rho = \frac{2A_p^2}{r_o^2 \lambda_f} \frac{C_p}{K_p^2}$$

Let

$$\alpha' = \frac{3A_o^2}{r_o^2 A_f} \text{ in cm} \tag{69}$$

Since

$$K_p = K - K_p \tag{71}$$

then

$$\rho/\alpha' = \frac{C_D}{(K - K_p)^2} \tag{86}$$

We have expressed ρ as ρ/α' in ohms since the constant α' can at best be estimated. Since the value of K_p at a given potential can be calculated by use of Equation 28 then the value of ρ/α' at a given potential can be determined. Such values of ρ/α' at a given potential ψ and ionic strength of KNO_3 for the various electrodes are listed in Tables 10 - 12. Plots of ρ/α' vs ψ at a given ionic strength of KNO_3 for the various electrodes are shown in Figures 13 - 15. Plots neglecting K_p were also made. Over the large part of the potential range studied K_p is small compared to K even if the Faradaic current is limited only by diffusion; if there is in addition any barrier to transfer of ions across the interface it is very likely that K_p would be negligible over the entire potential range studied. Such a barrier would behave formally as a resistor in series with the Faradaic capacitance. It may be sufficiently large that a negligible current passes through the Faradaic impedance, and hence the latter is insignificant.

The observed rapid rise in ρ/α' at very high negative potentials just where the Faradaic impedance due to I^- ion diffusion becomes

Figure 13. Dependence of resistivity of AgI on potential (relative to potential at zero point of charge)

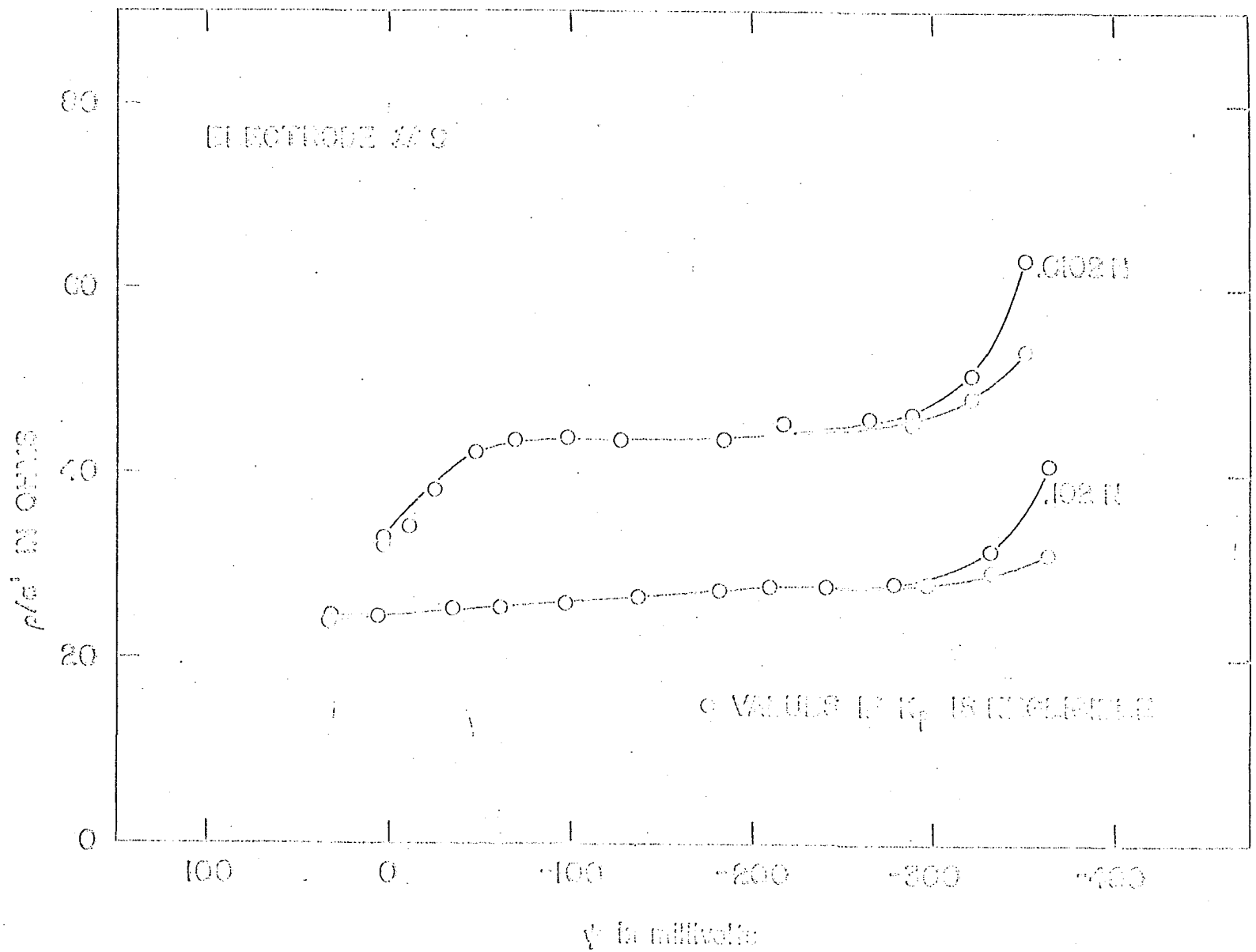
80
60
40
20
0
100
0
-100
-200
-300
-400
0.0021 N
.002 N

Figure 14. Dependence of resistivity of AgI on potential (relative to potential at zero point of charge)

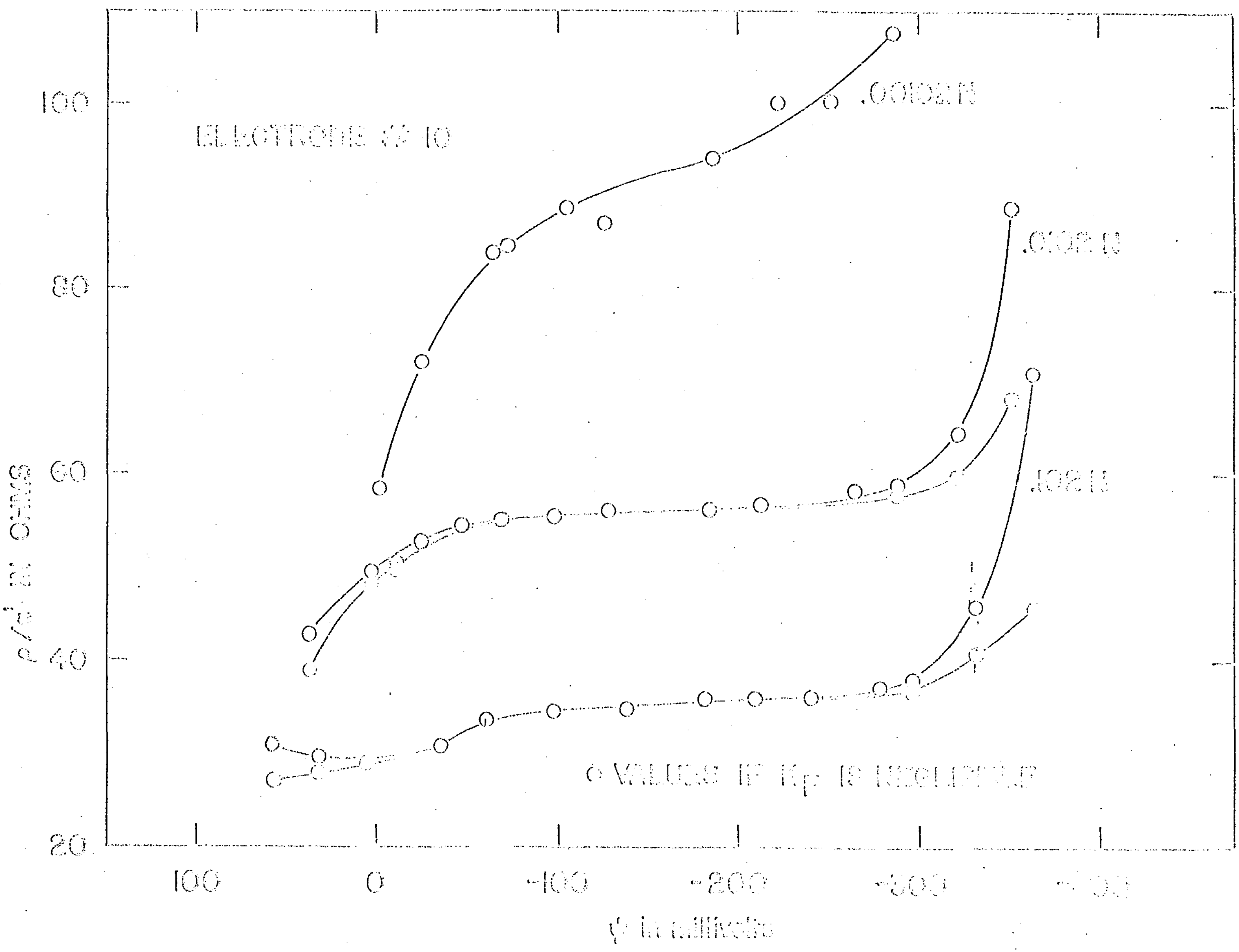
ELECTRODE # 10
o VALUES IF Rp IS NEGLIGIBLE
ρ/d in OHMS
ψ in millivolts
100
80
60
40
20
100
0
-100
-200
-300

Figure 15. Dependence of resistivity of AgI on potential (relative to potential at zero point of charge)

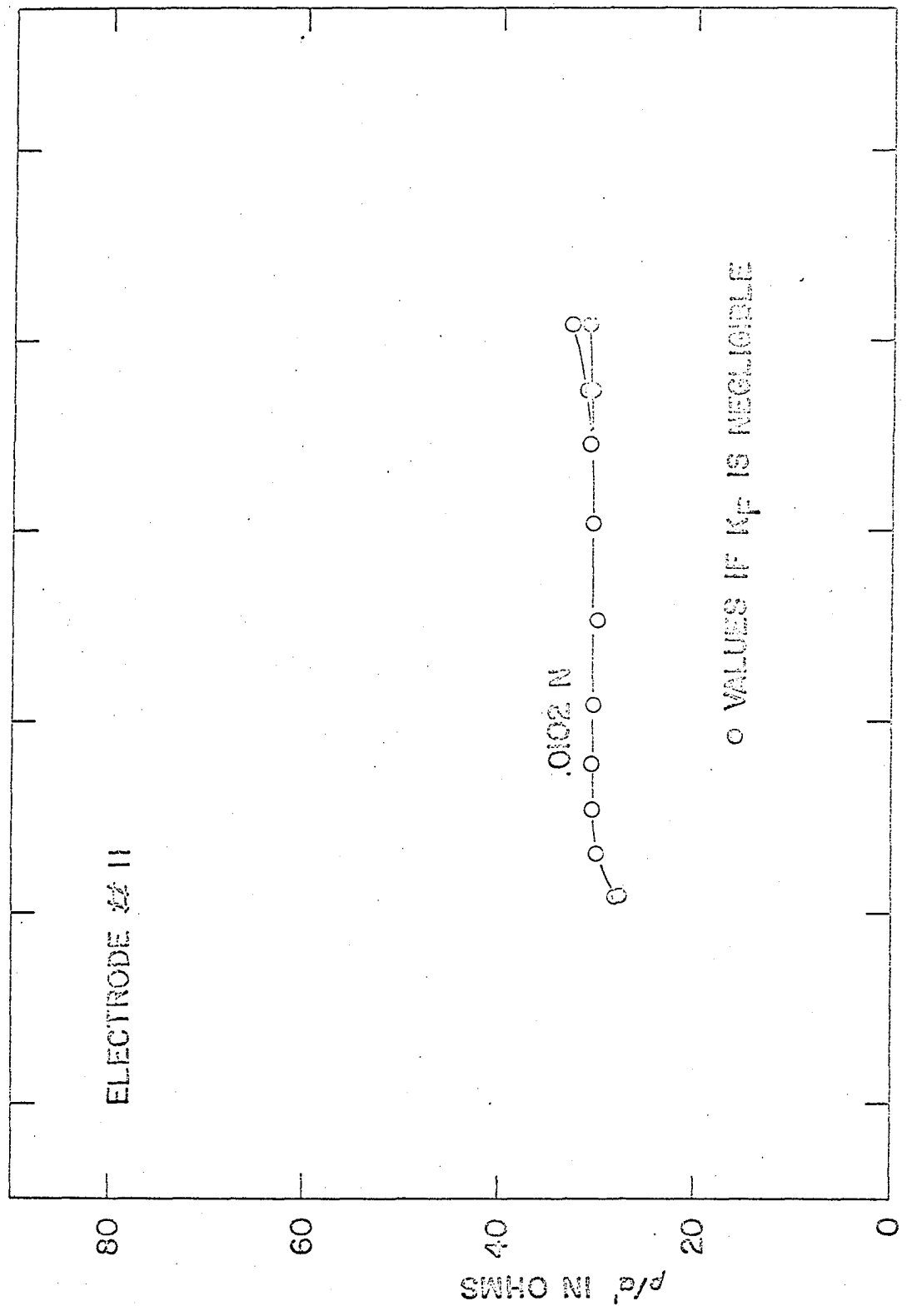
ELECTRODE # 11
.0102 N
o VALUES IF Kf IS NEGLIGIBLE
ρ/d' IN OHMS
ψ in millivolts
0
20
40
60
80
100
-100
-200
-300
-400

significant may be misleading. By neglecting K_p it is seen that only a slight rise in ρ/α' in this potential region occurs. This is more reasonable and hence suggests that a significant barrier to I^- transfer does occur. Experiments were not extended to sufficiently high positive potentials to permit conclusions regarding a possible barrier to Ag^+ transfer.

At first it may be thought that the observed increase in ρ/α' with decrease in ionic strength of solution is due to an increasing contribution by the electrolyte resistivity to the impedance of the pore. We had assumed it to be negligible compared to the AgI resistivity. An impedance formula was therefore derived permitting explicit inclusion of the solution resistivity. However, this formula predicted that ρ would vary with ionic strength in the range of ionic strengths studied in the opposite direction from that observed when the solution resistivity was significant. Perhaps the dependence of ρ/α' on ionic strength may be explained by the change in surface conditions with ionic strength. At any rate values of ρ/α' at the various ionic strengths tend to converge at positive potentials.

We can estimate the value of α' for an electrode as follows. We have

$$\alpha' = \frac{8A_p^2}{r_o^2 A_f} \tag{85}$$

Based on Equation 41b we estimate the radius of a pore to be

$$r_o \approx 10^{-5} \text{ cm}$$

We estimate the thickness τ of the AgI wall in the pore to be

$$\tau \approx 10^{-6} \text{ cm}$$

Hence

$$\alpha' \approx 8 \times 10^4 \frac{A_p^2}{A_D}$$

Using Table 9 we get for each electrode

$$\alpha'\#9 \approx 1.2 \times 10^4 \text{ cm}$$

$$\alpha'\#10 \approx .60 \times 10^4 \text{ cm}$$

$$\alpha'\#11 \approx .20 \times 10^4 \text{ cm}$$

We can estimate the value of ρ for an electrode as follows. Consider the value of ρ/α' for electrode #9 at $\psi = -11$ in .01N KNO_3 from Table 10. Using the above estimated value of α' for electrode #9 we get

$$\rho\#9 = 4.1 \times 10^5 \text{ ohm-cm at } \psi = -11 \text{ in .01N } KNO_3$$

Similarly

$$\rho\#10 = 3.0 \times 10^5 \text{ ohm-cm at } \psi = -11 \text{ for .01N } KNO_3$$

$$\rho\#11 = 5.6 \times 10^4 \text{ ohm-cm at } \psi = -9 \text{ for .01N } KNO_3$$

Note that we have assumed τ/r_o^2 has the same magnitude for each electrode. This assumption can at best be an approximation. The conductivity of AgI pellets at compressed pressures was studied recently by J. N. Mrgudich (15). He determined conductivity values of the order 10^{-4} to 10^{-5} $ohm^{-1}cm^{-1}$. The conductivity will partly depend on the impurity content of the specimen. Hence, the above magnitude and variation of resistivity among the various electrodes are reasonable.

The resistance R' of a AgI electrode can be estimated as follows. The solution resistance R_{sol} is expressed by

$$R_{sol} = K_{sol}\,\rho_{sol} \tag{87}$$

where ρ_{sol} is the resistivity of the solution and K_{sol} is the geometric proportionality constant in cm^{-1}. Throughout the experimental potential range the concentrations of Ag^+ and I^- are much less than that of the electrolyte KNO_3. Hence the solution resistivity is simply the electrolyte resistivity. The values of the resistivity of aqueous KNO_3 at 25°C at a given ionic strength are listed in Table 13. They were obtained from

Table 13. The values of the equivalent conductance in cm^2/ohm equivalent and resistivity ρ_{sol} in ohm-cm for KNO_3 at 25°C in water at various concentrations N in equivalents/liter

N	Λ	ρ_{sol}
.00102	141.8	6916
.01020	132.8	738.6
.10200	120.4	81.4

the American Institute of Physics Handbook (16). Using Equation 87 in Equation 81 we get

$$R_o = R' + K_{sol}\,\rho_{sol} \tag{88}$$

Since we observe that AgI resistivity ρ increases with decreasing ionic strength in the potential range studied then R' should vary similarly.

However, we can consider R' to be constant as an approximation for the ionic strengths studied. Hence a plot of the R_o vs ρ_{sol} is approximately linear with an intercept approximately R'. A two point plot of R_o vs ρ_{sol} for electrodes #9 and #10 using data at .1N and .01N solution was made. We determine

$$R' \approx 26 \text{ ohms for electrode \#9}$$

$$R' \approx 29 \text{ ohms for electrode \#10}$$

The effective thickness of AgI on the electrode can be estimated once R' is estimated. We have

$$R' = \frac{\rho \tau_{eff}}{A_e} \tag{77}$$

Using the above estimated values of ρ and R' and Table 1 we get

$$\tau_{eff} \approx 2.4 \times 10^{-6} \text{ cm for electrode \#9}$$

$$\tau_{eff} \approx 3.5 \times 10^{-6} \text{ cm for electrode \#10}$$

Comparing these values with the thickness τ_e of AgI we find

$$\frac{\tau_{eff}}{\tau_e} \approx .70 \times 10^{-2} \text{ for electrode \#9}$$

$$\frac{\tau_{eff}}{\tau_e} \approx .80 \times 10^{-2} \text{ for electrode \#10}$$

These small ratios indicate that very deep pores occur and explain why the resistance R' in AgI is small compared to the electrolyte resistance for the electrolyte concentrations studied.

The Capacitance C' of Solid Silver Iodide

Plots of the equivalent capacitance C' of AgI vs potential ψ for the various electrodes are shown in Figures 16 - 18.

The observed rise in capacitance C' at positive potentials and very high negative potentials suggests that capacitance C' is approximately a diffuse capacitance with mobile impurities as given by Equation 75'. Note that C' should be plotted vs $V_c(o)$, the potential just inside the crystal surface relative to the crystal bulk, rather than potential ψ. The potential at which the minimum of capacitance C' occurs is about ψ = -240 millivolts for electrodes #9 and #10 at the various electrolyte concentrations. The potential at which the minimum of capacitance C' occurs for electrode #11 cannot be detected with accuracy but is in the range between ψ = -240 millivolts and ψ = -280 millivolts. A comparison of the C' and C_D values for a given electrode shows that the former is large compared to the latter.

Since capacitance C' changes rapidly around the zero point of charge so also must the potential $V_c(o)$. This is also the case at very high negative potentials ($|\psi| \geq$ 300 mv). The observed slight variation of capacitance C' between ψ = -100 mv and ψ = -300 mv indicates that potential $V_c(o)$ does likewise in this region.

For studies of the impedance of solid Ag cl and solid Ag Br see references 17 and 18 respectively.

Figure 16. Dependence of equivalent series capacitance of solid AgI on potential (relative to potential at zero point of charge)

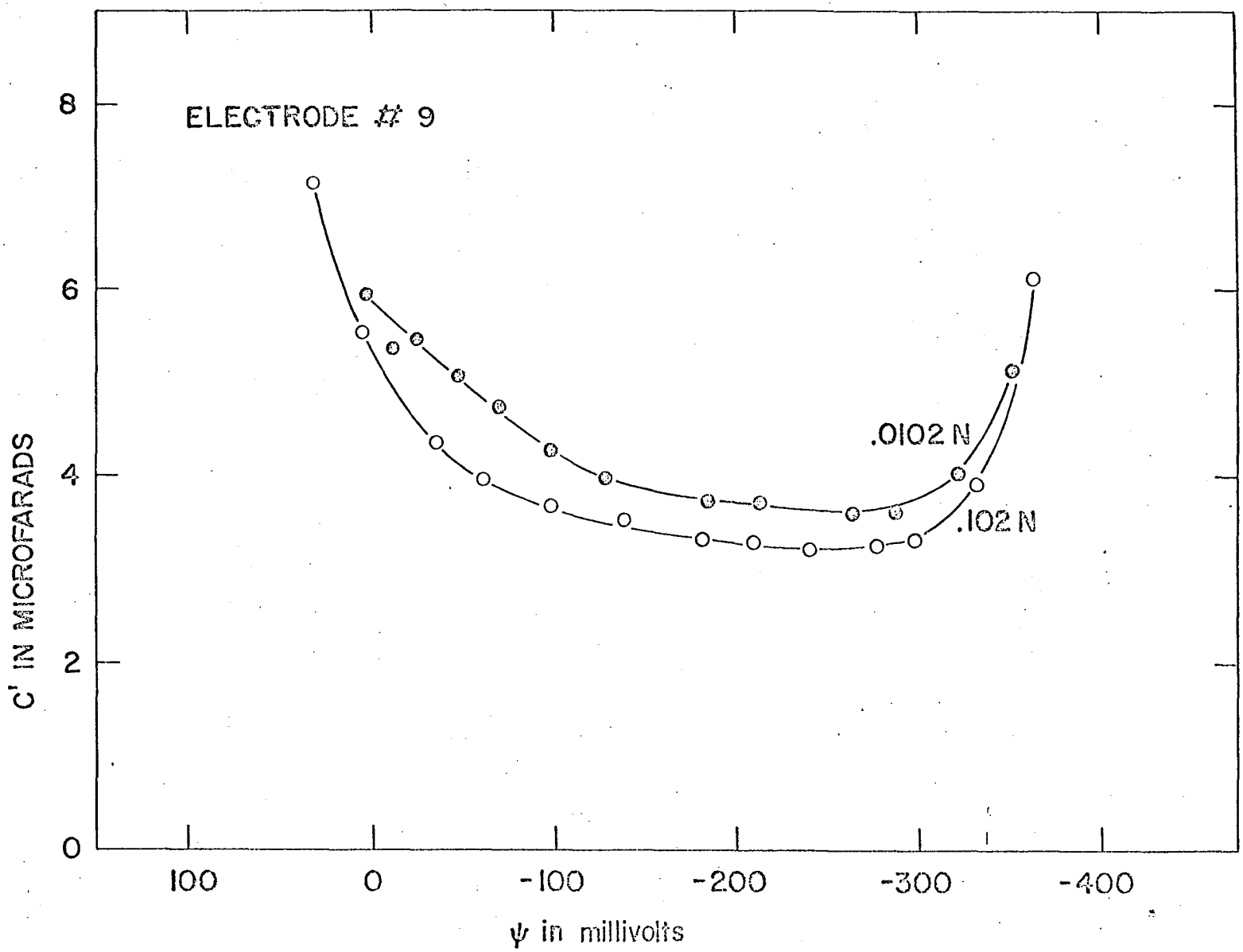
ELECTRODE # 9
.0102 N
.102 N
C' IN MICROFARADS
8
6
4
2
0
100
0
-100
-200
-300
-400
ψ in millivolts

Figure 17. Dependence of equivalent series capacitance of solid AgI on potential (relative to potential at zero point of charge)

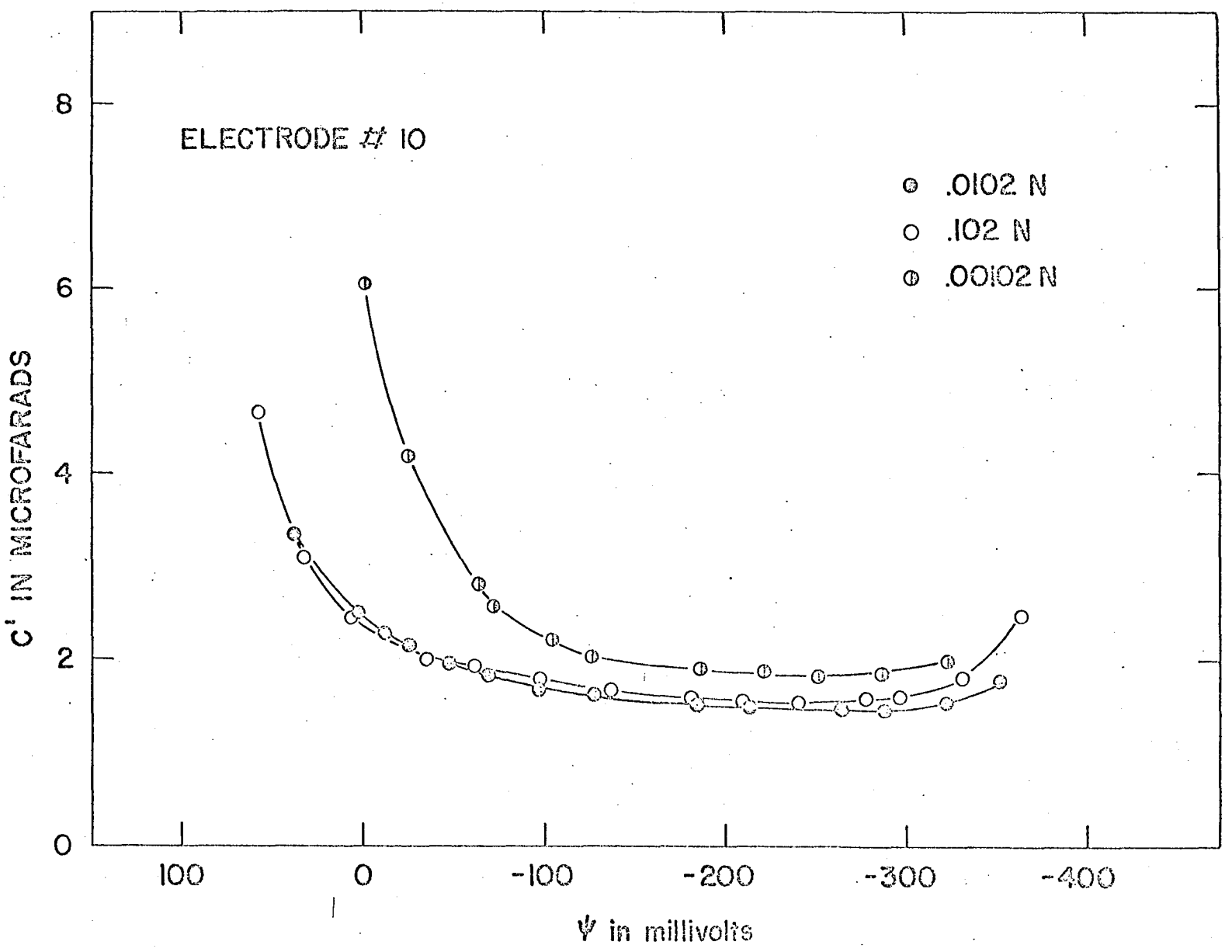
ELECTRODE # 10
.0102 N
.102 N
.00102 N
C' IN MICROFARADS
0
2
4
6
8
100
0
-100
-200
-300
-400
Ψ in millivolts

Figure 18. Dependence of equivalent series capacitance of solid AgI on potential (relative to potential at zero point of charge)

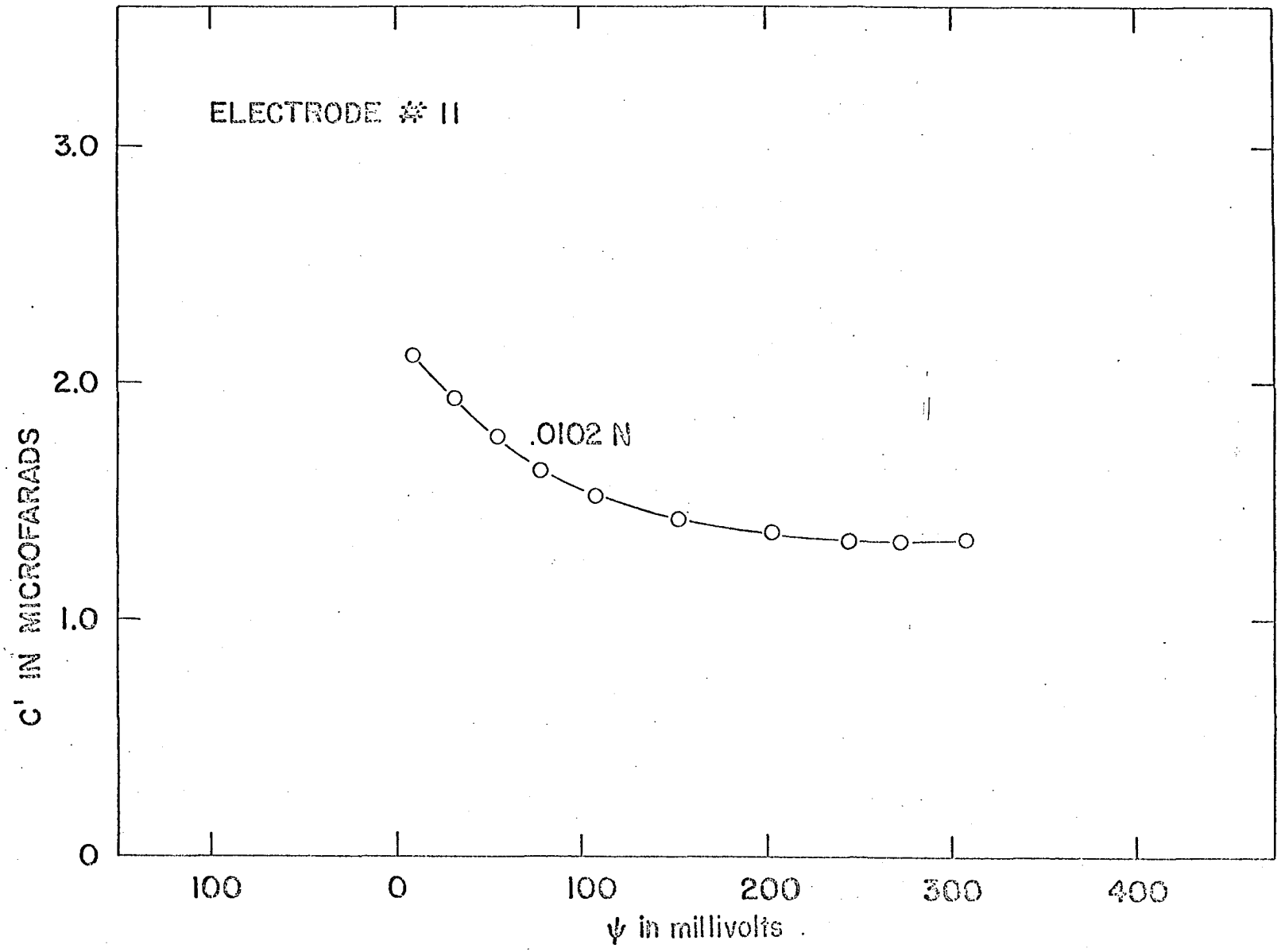
ELECTRODE # 11
.0102 N
C' IN MICROFARADS
3.0
2.0
1.0
0
100
0
100
200
300
400
ψ in millivolts

SUMMARY

An impedance bridge was used to determine the equivalent series capacitance C_V and resistance R_V for the AgI-aqueous solution system. An AgI electrode in contact with an aqueous potassium nitrate solution containing a very dilute concentration of Ag^+ and I^- ions served as the system. A cell potential range of about 420 millivolts was used at KNO_3 concentrations of .1N, .01N, and .001N. The C_V and R_V values at a given potential and electrolyte concentration were determined in a frequency range from 256 cycles per second to 9,168 cycles per second. Several electrodes of varying AgI thickness were studied to check the consistency of the results. An electrical analog circuit was proposed for the interface which was consistent with known properties of this interface and which adequately represented the dependence of C_V and R_V on frequency and potential over the ranges of frequency and potential studied.

It has been shown that the frequency dependences of both C_V and R_V are due to distributed capacitances in the pores of AgI. This effect can be described by tapered RC transmission lines connected in parallel. The equivalent capacitance and resistance of one line represents the impedance in one pore. The equivalent capacitance C_P and resistance R_P of the parallel transmission lines is in parallel with the differential capacitance C_D of the double layer associated with the flat portion of the AgI. The resulting impedance is in series with both the series equivalent capacitance C' and resistance R' of solid AgI and the solution resistance. Capacitance C' arises from space charges of defects in the AgI.

By setting the value of the AgI double layer capacity equal to that for the mercury-sodium fluoride solution interface at the zero point of charge at .001N solution the area of the flat portion of the AgI electrode is determined, and hence the AgI double layer capacity at any potential and electrolyte concentration. This was the goal of our research. We find that the double capacity values agree very well with those of Agar around the zero point of charge at various electrolyte concentrations. Whereas his values decrease slightly at high negative potentials we observe increased values in this potential range.

SUGGESTIONS FOR FUTURE WORK

An investigation may be undertaken to use various electrolytes so that differences in the AgI double layer capacity can be determined. Such differences would occur in the Stern layer for ions of the same valence. Such work has been done by J. Lyklema (9) by the titration method. He observed that the double layer capacity varied somewhat in the negative potential region for various cations.

An investigation with the use of an organic solvent may be undertaken. The Stern capacity should change from that with water as the solvent due to differences in dielectric constant. The dielectric constant in the Stern layer has been estimated to range between 4 and 10 with water as the solvent and hence a drop by at least a factor of 8 from bulk conditions.

The effect of different methods of preparing the AgI electrode may also be studied.

A study using an electrolyte concentration of 1N should be tried. A significant difference between those values and those at .1N would indicate that specific adsorption occurs. The very small electrolyte resistance in this case would also permit a more accurate measurement of the AgI resistance.

BIBLIOGRAPHY

1. Stern, O. Z. Electrochem. 30: 508. 1924.

2. Grahame, D. C. Chem. Revs. 41: 441. 1947.

3. Frumkin, A. and Proskurnin, M. Trans. Far. Soc. 31: 110. 1935.

4. Grahame, D. C. J. Am. Chem. Soc. 71: 2975. 1949.

5. Laar, J. A. W. Van. Unpublished Ph.D. Thesis. Utrecht, The Netherlands, Library, State University of Utrecht. 1952.

6. Mackor, E. L. Rec. Trav. Chim. 70: 663. 1951.

7. _____ Rec. Trav. Chim. 70: 763. 1951.

8. Lyklema, J. and Overbeek, J. Th. G. J. Colloid Science 16: 595. 1961.

9. _____ Trans. Far. Soc. 59: 418. 1963.

10. Agar, G. The adsorption of amine on silver iodide. Unpublished Ph.D. Thesis. Cambridge, Massachusetts, Library, Massachusetts Institute of Technology. 1961.

11. Kelsh, D. The deformation of the electrocapillary curve due to adsorption of organic molecules. Unpublished Ph.D. Thesis. Ames, Iowa, Library, Iowa State University of Science and Technology. 1962.

12. De Levie, R. Electrochim. Acta 8: 751. 1963.

13. _____ Electrochim. Acta 9: 1931. 1964.

14. Iwasaki, I. and DeBruyn, P. L. J. Phys. Chem. 62: 594. 1958.

15. Mrgudich, J. N. J. Electrochem. Soc. 107: 475. 1960.

16. Gray, D. E. American Institute of Physics Handbook. 2nd ed. McGraw-Hill Book Co., Inc., New York, N.Y. 1963.

17. Steidel, C. A. The impedance at the AgCl-aqueous solution interface. Unpublished Ph.D. Thesis. Ithaca, New York, Library, Cornell University. 1966.

18. Rayleigh, D. O. J. of Phys. Chem. 70: 689. 1966.

ACKNOWLEDGEMENTS

The author gratefully acknowledges the reliable support and understanding of Professor R. S. Hansen during the course of this research. He suggested the problem and was very helpful in working out clear theoretical treatments.

Special thanks also goes to Robert Frost, who wrote the program to determine the various experimental parameters on the I.B.M. 360/50 computer. His willingness to encounter and solve the program problems that arose is much appreciated.

The experimental groundwork performed by Daniel Grantham with the impedance bridge was of great benefit to the author.